

Towards Nanotubular Structures with Large Voids: Dynamic Heteroleptic Oligophenanthroline Metallonanoscaffolds and their Solution-State Properties

Michael Schmittel,^{*,[a]} Venkateshwarlu Kalsani,^[a, d] Christoph Michel,^[a] Prasenjit Mal,^[a] Horst Ammon,^[b] Frank Jäckel,^[c, e] and Jürgen P. Rabe^[c]

Abstract: The assembly of a rigid macrocycle with two exotopic phenanthroline binding sites in combination with linear bis- or trisphenanthrolines and copper(I) ions is used to generate nanoscale double and triple deckers, the latter showing a tubular structure. With supramolecular chemistry expanding to dynamic, large cavity, nano-

scale structures, it becomes increasingly important to use robust assembly protocols as well as reliable characteriza-

Keywords: coordination chemistry · copper · nanostructures · self-assembly · supramolecular chemistry

tion techniques. To fully elucidate and to describe the dynamic nature of metallonanoscaffolds with large voids, we applied a battery of both direct and indirect solution-state characterization methods. These methods along with the conventional direct methods provide a very useful tool for characterizing tubular nanoscaffold aggregates.

Introduction

While the elaboration of reliable and robust self-assembly protocols for supramolecular structures has been a major focus of the last two decades,^[1] there is now mounting interest in the engineering of discrete aggregates at the >3 nm scale. Leading pioneers in the field, such as Stang,^[2] Lehn,^[3] Newkome,^[4] Reinhoudt,^[5] Fujita,^[6] Kobuke,^[7] and others,^[8]

have reported on sparkling nanoscale architectures, for example, polygons/polyhedra, rosette aggregates, and porphyrin arrays. However, not all of the above cited nanoarchitectures, are dynamic, as expected for truly supramolecular systems.^[1a] Consequently, there is rather little detailed information reported in the literature on the specific dynamic properties of discrete assemblies >3 nm in size. Due to the dynamics, large size, and huge voids, their characterization causes unusual problems, both in solution and the solid state. As they contain a multitude of disordered solvent molecules, suitable single-crystals for X-ray diffraction measurements are difficult to obtain,^[2-5,8] but, even if they are accessible, these data do not convey any information about the solution structure and the dynamic nature. Ancillary methods,^[9] like scanning probe microscopy techniques^[9a,b,d] and high-resolution TEM (HRTEM),^[9c] have also shown some utility, but again they do not disclose information about dynamic properties. Consequently, an encompassing understanding of dynamic nanostructures requires results from a variety of complementary solution-state characterization protocols.

Traditional methods for characterizing aggregates include solution-state techniques (NMR and UV/Vis spectroscopy, and mass spectrometry) in combination with evaluation tools, such as Job plots or Scatchard plots. More recent techniques, such as DOSY-NMR spectroscopy^[10] and analytical ultracentrifugation,^[11] equally provide valuable information


[a] Prof. Dr. M. Schmittel, Dr. V. Kalsani, Dr. C. Michel, Dr. P. Mal
Center of Micro and Nanochemistry and Engineering
Organische Chemie I, Universität Siegen
Adolf-Reichwein-Str. 2, 57068 Siegen (Germany)
Fax: (+49)271-740-3270
E-mail: schmittel@chemie.uni-siegen.de

[b] Dr. H. Ammon
Institut für Organische Chemie der Universität Würzburg
Am Hubland, 97074 Würzburg (Germany)

[c] Dr. F. Jäckel, Prof. Dr. J. P. Rabe
Humboldt University Berlin, Department of Physics
Newtonstrasse 15, 12489, Berlin (Germany)

[d] Dr. V. Kalsani
Present address: Department of Chemistry, Tufts University
Medford, MA 02155 (USA)

[e] Dr. F. Jäckel
Present address: Department of Chemistry, Stanford University
Stanford, CA 94305 (USA)

 Supporting information for this article is available on the WWW under <http://www.chemeurj.org/> or from the author.

about the integrity of the assemblies. In a few cases, vapor-phase osmometry has also been used, but widespread use is prohibited by the large sample concentration required and the low molecular-mass range.^[12] However, in most cases these techniques serve to establish the structural integrity of the nanostructure more than to evaluate the dynamic properties as such.

In the following, we describe the preparation of tubular heteroleptic oligophenanthroline metallonanoscaffolds, and our efforts to elucidate their structural integrity and dynamic properties. The tubular structure was set up by the utilization of a rather sturdy macrocyclic building block in combination with a pillarlike oligophenanthroline. The indispensable labile heteroleptic metal unit was conceived on the basis of the HETPHEN concept,^[13] which suggested the utilization of copper(I) bisphenanthroline complexes,^[14] since they show high thermodynamic stability, well-defined geometry, and kinetic lability. Indeed, the combined use of HETPHEN concept, maximum site occupancy, and cooperativity led quantitatively to nanoscale metallosupramolecular assemblies, some of which have been described in an earlier communication.^[13d] Extension to systems of almost 5 nm length is now reported for the first time using linear bis- and tri-phenanthrolines (**1a–h** and **2**). All aggregates were formed under thermodynamic control in rapid equilibrium at room temperature. As these systems did not yield meaningful X-ray, AFM, and HRTEM data, solution-state characterization became most important. Apart from conventional NMR spectroscopic and mass spectrometric characteriza-

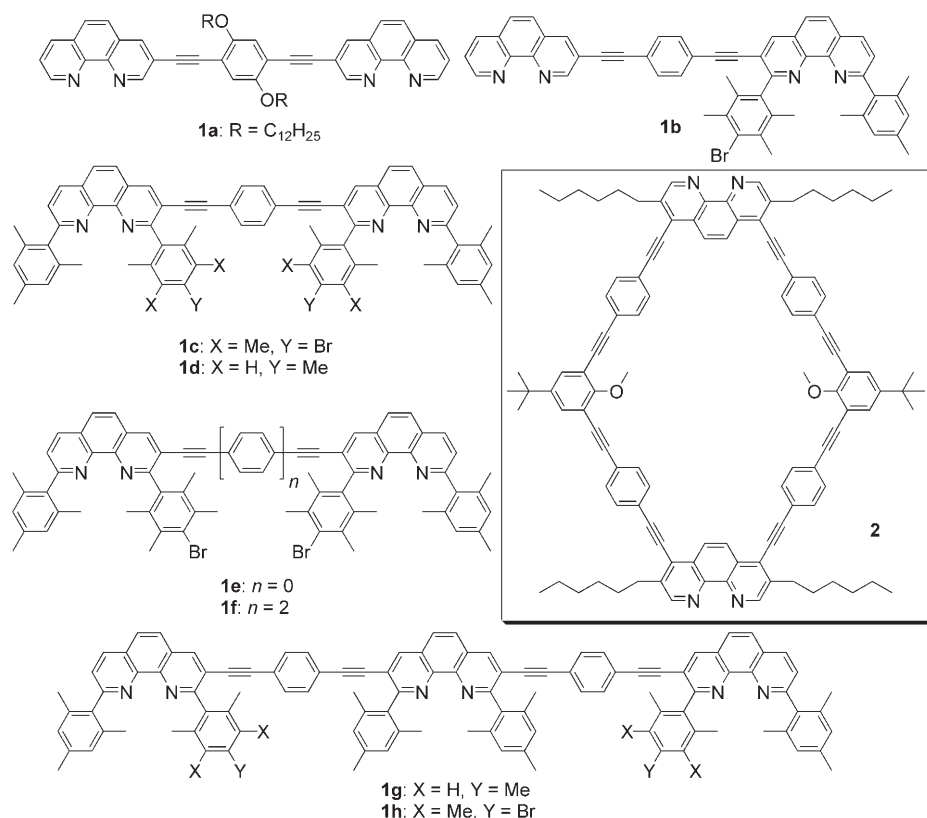
tion, we outline the use of analytical ultracentrifugation and DOSY-NMR spectroscopy to elucidate the structure, size, and solvent content of the proposed nanoedifices. Further control experiments, such as oxidation, ligand/metal exchange studies, and size selectivity studies were performed to increase our understanding of the proposed structures and their dynamic interconversion. In addition, the fruitful combination of ESI-MS and UV/Vis spectroscopy allowed characterization of various intermediates on the route to the final assemblies.

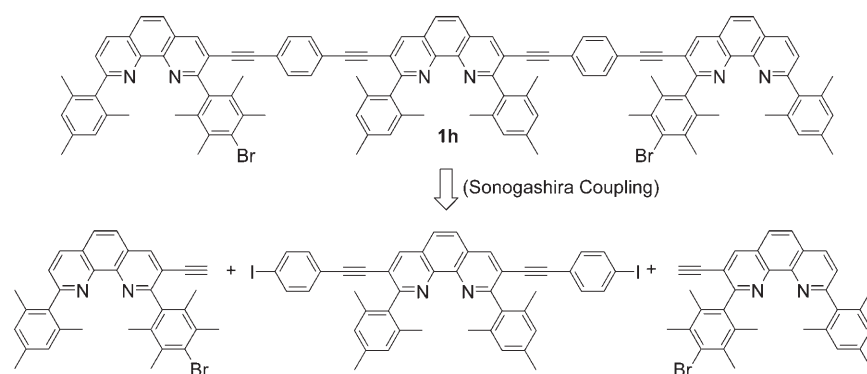
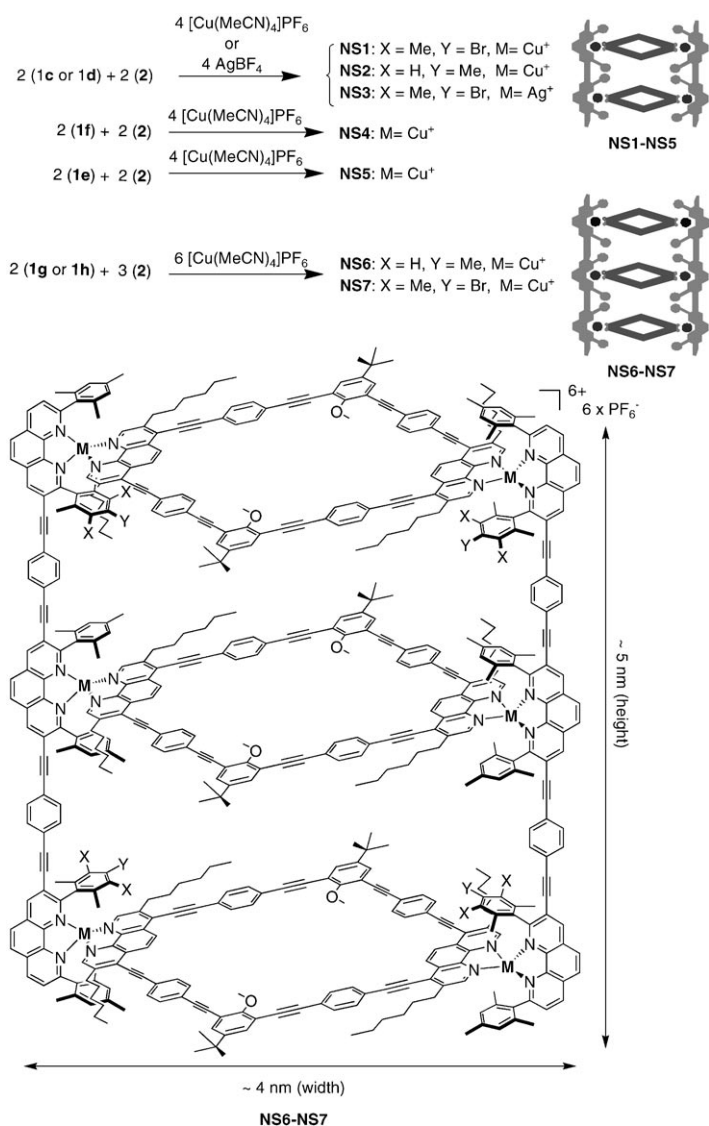
Results

Assembly of nanoscaffolds:

Preparation of ligands: The ligands^[15] used for the present study (**1a–h**, **2**) are depicted above; these ligands (except for **1a,b**) were conceived according to the HETPHEN concept.^[13] Scheme 1 depicts the retrosynthetic analysis for the so far unknown ligand **1h**. The synthesis was achieved following a procedure reported by our group.^[15]

Assembly: In the present approach ligands **1** were combined with the macrocyclic ligand **2** in the presence of the appropriate amount of copper, delivered as [Cu(MeCN)₄]PF₆. According to our general protocol,^[13d] the simple mixing of **1**, **2**, and [Cu(MeCN)₄]PF₆ (**1c–f**/2/[Cu(MeCN)₄]PF₆ = 2:2:4 (**NS1**, **NS2**, **NS4**, **NS5**) or **1g,h**/2/[Cu(MeCN)₄]PF₆ = 2:3:6 (**NS6**, **NS7**)) yielded dark red nanoscaffolds in virtually quantitative yields (Scheme 2). As a proof of principle, the faint yellow silver nanoscaffold **NS3** was made from **1c**/2/AgBF₄ = 2:2:4. The assemblies proved to be stable for more than a year and soluble in a variety of solvents, such as dichloromethane, acetonitrile, nitromethane, dimethylformamide, and dimethylsulfoxide. Complexation of the non-HETPHEN ligands **1a** or **1b** under the same conditions (with **2** and copper(I)) was expected to yield nanoscale heteroleptic metallo assemblies similar to **NS1–NS5**. However, their reaction afforded a variety of homoleptic and heteroleptic combinations. Clearly, there is a need for additional control to drive this equilibrium toward a single heteroleptic nanostructure as achieved by the use of the HETPHEN concept.



Scheme 1. Retrosynthetic analysis for ligand **1h**.Scheme 2. Metal-mediated assembly of nanoscaffolds **NS1–NS7**.

Standard characterization protocols

NMR spectroscopy: ^1H NMR spectra exhibited a single set of sharp signals indicative of a highly symmetric species. As

already seen earlier in analogous mononuclear complexes, the mesityl protons in **NS1–NS7** showed a distinctive high-field shift to around $\delta=6$ ppm (e.g., $\delta=6.11$, 6.10, 6.06/5.97 and 6.02–5.99 ppm for **NS4**, **NS5**, **NS6**, and **NS7**, respectively) relative to those in the free ligands (e.g., in **1h**, $\delta=6.9$ –7.0 ppm), characteristic for heteroleptic complex formation.^[13] Similar results were obtained for the mesityl protons in the silver nanoscaffold **NS3** ($\delta=5.96$ ppm).

UV/Vis spectroscopy: The UV/Vis absorption spectra of **NS1–NS7** can also be utilized for characterization. As representative examples the absorption spectra of the heteroleptic nanoscaffolds **NS6** and **NS7** are depicted in Figure 1 (see Supporting Information for **NS1–NS5**). The strong absorption bands at 250–400 nm correspond to ligand π - π^* transitions,^[16] whereas the absorption band at ≈ 500 nm was assigned to the metal-to-ligand charge-transfer (MLCT) transition, being responsible for the red color. For all copper(I) nanoscaffolds **NS** the MLCT band is almost identical, indicative of a very similar environment at the metal centers in all the assemblies. Moreover, the absorptions are very similar to those of analogous heteroleptic copper(I) grid assemblies.^[17] The MLCT bands in the visible region at $\lambda=499$ nm for **NS6** and **NS7** ($\epsilon_{\text{max}}=65\,640$ and $60\,880\text{ M}^{-1}\text{ cm}^{-1}$) represent six copper(I) bisphenanthroline complex units. In comparison, in bis(2,2'-bipyridine) copper complexes, MLCT bands with $\epsilon_{\text{max}}=6800$ – $8500\text{ M}^{-1}\text{ cm}^{-1}$ are typical, while those for bisphenanthroline copper complexes amount to 3200 – $13\,200\text{ M}^{-1}\text{ cm}^{-1}$.^[18]

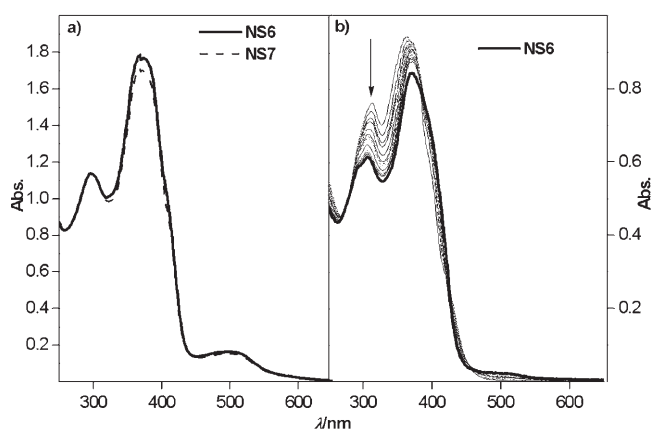
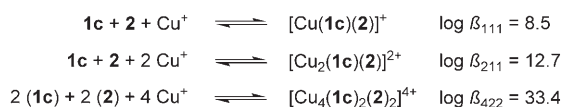


Figure 1. a) UV/Vis absorption spectra of **NS6** and **NS7** at $2.5 \times 10^{-6}\text{ M}$ in DCM at 25°C . b) Change of the absorption spectra of a mixture of **1g** ($1.25 \times 10^{-6}\text{ M}$) and **2** ($1.875 \times 10^{-6}\text{ M}$) upon progressive addition of $[\text{Cu}(\text{MeCN})_4]\text{PF}_6$ ($5 \times 10^{-4}\text{ M}$) until the correct stoichiometry was reached. The bold line represents the spectrum after final formation of **NS6**.

To get a comprehensive account for the formation of the nanoscaffolds, **1c** and **2** were titrated with aliquot amounts of $[\text{Cu}(\text{MeCN})_4]\text{PF}_6$ in dichloromethane (DCM) at 25 °C, resulting in significant changes in the UV/Vis spectra (Supporting Information). Scheme 3 displays the binding con-



Scheme 3. Overall stability constants of various complexes and **NS1** obtained from the titration of **1c** and **2** with aliquot amounts of $[\text{Cu}(\text{MeCN})_4]\text{PF}_6$ in dichloromethane.

stants obtained for the formation of various intermediates and of **NS1**. Distribution curves were computed (Figure 2) from these results. The Scatchard plot suggests a strong posi-

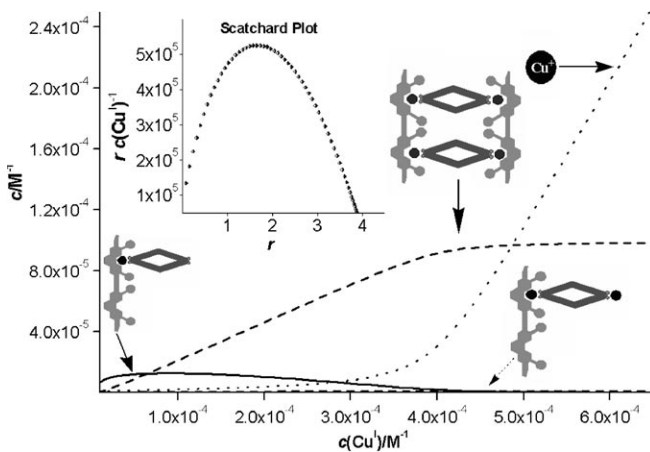


Figure 2. Distribution curves, as derived from the stability constants in Scheme 3, of various copper(I) complexes $[\text{Cu}_n(\mathbf{1c})_b(\mathbf{2})_c]^{n+}$ plotted against the concentration of copper(I). Solvent: DCM; $T=25^\circ\text{C}$. The inset shows a Scatchard plot (r = ratio of the concentration of bound copper(I) to total available binding sites; $c(\text{Cu}^+) = \text{conc. of free copper(I)}$).

tive cooperativity^[18b] in the formation of the heteroleptic nanoscaffold. Only two intermediates were formed in very minor amounts. This observation is in line with the ESI-MS results (vide infra). During the very early stages of the titration, complex $[\text{Cu}(\mathbf{1c})(\mathbf{2})]^+$ was formed as the major species serving as precursor to $[\text{Cu}_2(\mathbf{1c})(\mathbf{2})]^{2+}$, as detected by ESI-MS. According to the species distribution curves, as soon as $[\text{Cu}_2(\mathbf{1c})(\mathbf{2})]^{2+}$ was formed, **NS1** was rapidly assembled in a final dimerization step.

Furthermore, we intensely monitored the changes in the UV/Vis absorption behavior of linear phenanthroline **1g**, macrocycle **2**, and a 1:1 mixture of **1g** and **2** upon titration with $[\text{Cu}(\text{MeCN})_4]\text{PF}_6$. Isosbestic points in the titrations of **1g** or **2** with copper(I) are readily observed (Figure 3). As can be visualized from the titration of **1g** depicted in Figure 3a, a new absorption band emerged at approximately 410 nm due to the triply coordinated trisphenanthroline,

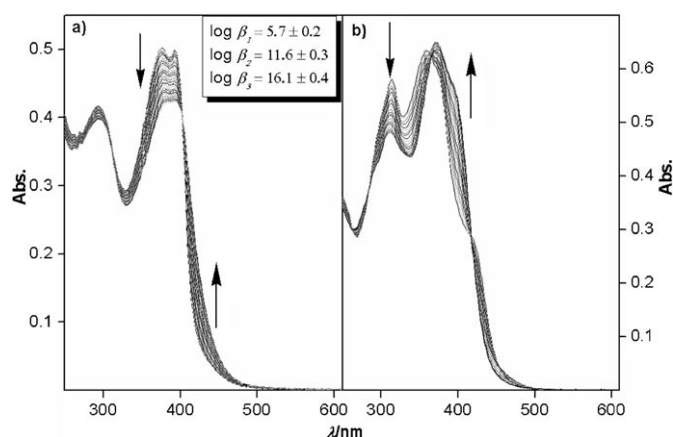


Figure 3. a) Change in the absorption spectra of **1g** ($5.0 \times 10^{-6} \text{M}$) upon progressive addition of $[\text{Cu}(\text{MeCN})_4]\text{PF}_6$ ($1.0 \times 10^{-3} \text{M}$). Stability constants for $[\text{Cu}_n(\mathbf{1g})]^{n+}$ are shown in the inset. b) Change in the absorption spectra of **2** ($7.5 \times 10^{-6} \text{M}$) upon progressive addition of $[\text{Cu}(\text{MeCN})_4]\text{PF}_6$ ($1.0 \times 10^{-3} \text{M}$).

$[\text{Cu}_3(\mathbf{1g})]^{3+}$. The absorption is quite distinct from the characteristic MLCT band of **NS6** at $\approx 499 \text{nm}$. Secondly, Figure 3b represents the absorption spectra of **2** in the presence of different copper(I) ion concentrations. Apparently, the different species are in full equilibrium, since the absorption changes take place through three clear isosbestic points. This was further established from the analysis of ESI-MS spectra (Supporting Information). The kinetics are different for the titration of **1g** and **2** with $[\text{Cu}(\text{MeCN})_4]\text{PF}_6$ (Figure 1b). As seen from the figure, initially the changes in absorption took place through isosbestic points, clearly indicating that all species are in equilibrium. Interestingly, however, after completion of the addition of copper(I) the new absorption band of **NS6** appeared slowly. Apparently, nanoscaffold **NS6** is thermodynamically stable, but does not form as rapidly as $[\text{Cu}_3(\mathbf{1g})]^{3+}$ or **NS1**. The fact that the absorption band due to **NS6** does not pass through the isosbestic points indicates that some of the readily formed intermediate complexes do not directly lead to **NS6**, but only after error correction.

In concluding the UV/Vis titration part, a rapid four-step process was proposed for the formation of the eight-piece heteroleptic nanoscaffold assembly **NS1** on the basis of the above titration data, while **NS6** only assembled after error correction (vide supra). These results demonstrate the exciting potential of the HETPHEN concept for the quantitative construction of heteroleptic supramolecular architectures.

ESI mass spectrometry (MS): ESI-MS is one of the important methods for elucidating metallosupramolecular structures in solution.^[19] ESI-MS analysis of **NS1–NS7** confirmed the clean formation of the proposed heteroaggregate structures, as demonstrated in Figures 4 and 5 (for **NS1** and **NS6**, respectively). Clearly, the ESI-MS spectrum of **NS1** only shows two signal groups in between $m/z=200$ and 2000, which can both be assigned to the nanostructure. The signals correspond to $[\text{NS1}-4\text{PF}_6]^{4+}$ ($m/z=1391.5 \text{Da}$), and

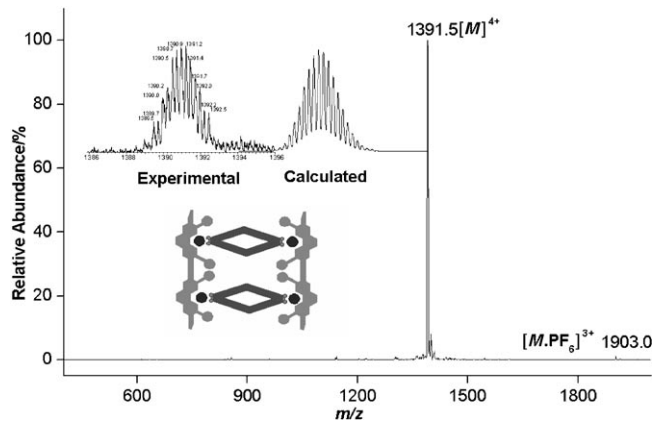


Figure 4. ESI-MS of **NS1**: the inset shows the experimental isotopic distribution for the 4+ charged species along with its calculated one.

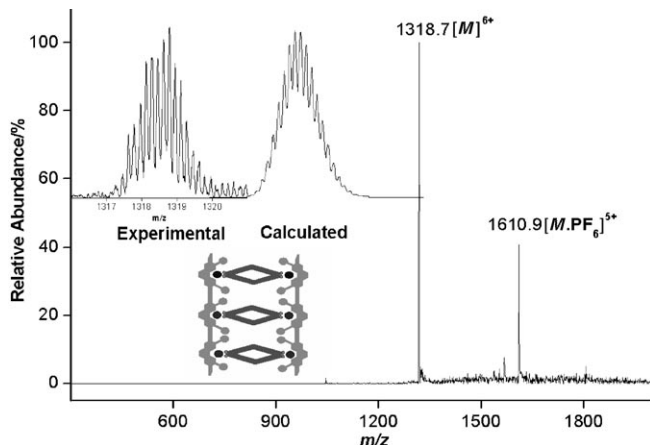


Figure 5. ESI-MS of **NS6**: the inset shows the experimental isotopic distribution for the 6+ charged species along with its calculated one.

[**NS1**–3PF₆]³⁺ (*m/z* 1903.0 Da). The signals of the linear ligand **1c** or macrocycle **2** were not visible. The ESI-MS spectrum analysis of **NS6** afforded signals for [**NS6**–6PF₆]⁶⁺ (*m/z* 1318.7 Da) and [**NS6**–5PF₆]⁵⁺ (*m/z* 1610.9 Da). As for **NS1**, the ESI-MS spectrum of **NS6** is also free of signals from the ligands. The nanoscaffolds were found to be quite stable under ESI conditions, since no fragments were observed, even at higher voltages. The experimental isotopic distributions (black lines) are in very good agreement with the calculated distributions (gray lines). Similar results were obtained for all other nanoscaffolds (see Supporting Information). Elemental analyses and high-resolution ESI of the assemblies were also in good agreement with the proposed composition.

ESI-MS assignments were further confirmed by collisional fragmentation experiments. Fragmentation of **NS1**⁴⁺ produced the signal corresponding to [Cu₂(**1c**)(**2**)²⁺ with its isotopic distribution being in good agreement with the proposed composition (Supporting Information).

DOSY NMR spectroscopy: Stang^[2a] and Cohen^[10] have utilized ¹H NMR diffusion experiments to investigate the hydrodynamic radius of nanoscale aggregates. In contrast, analytical ultra-centrifugation can provide much more detailed information, as will be shown below. We determined the diffusion coefficients for nanoscaffolds **NS1** and **NS6** in [D₂]dichloromethane, which were in agreement with the structural assignment.

Analytical ultracentrifugation (AUC): Though AUC has recently become a recommended technique to study the solution integrity of metallocsupramolecular assemblies, very few reports have been given that utilize this method.^[20] Such investigations are very useful, not only to obtain the molar mass and hydrodynamic radius of the aggregates, but also to gather vital information about the number of solvent molecules associated with the supramolecular aggregates. Sedimentation velocity experiments on **NS2** in acetone illustrated clearly that only one single species existed in solution at ambient temperature. From the density variation in two different solvents (acetone and [D₆]acetone) a dry molar mass of 5831 g mol⁻¹ was obtained. This is in admirable concord (±1%) with the calculated mass for **NS2** of 5772 g mol⁻¹. Moreover, the experimental hydrodynamic diameter of 4.2 nm is in superb agreement with the calculated size of the nanoscaffold (the diagonal distance between two copper centers amounts to 3.6 nm, the full diagonal (between the two terminal phenanthrolines) amounts to 4.7 nm). From sedimentation velocity experiments, a molecular mass for the solvated nanoscaffold of 19.8 × 10³ g mol⁻¹ was derived (Supporting Information), which suggests a solvation of 2.44 g g⁻¹.

AFM investigations of NS1: Recently, atomic force microscopy (AFM) has been used to image discrete molecular nanostructures.^[7b] Encouraged by these reports, imaging of single **NS1** by using the AFM tapping mode was attempted under ambient conditions.^[21] Samples were prepared by spincoating solutions of **NS1** in trichlorobenzene at various concentrations onto substrates of freshly cleaved mica, which were rinsed with milliQ-water and subsequently dried in a nitrogen flow. Estimated concentrations ranged from ≈10⁻³ M down to ≈10⁻¹⁰ M. Figure 6a displays the height images of samples prepared from different **NS1** concentrations. At high concentrations a distribution of large aggregates was observed. Dilution reduced both the number and the size of the aggregates. Figure 6b and c display histograms of the height and lateral dimensions of the objects (corrected for the tip broadening effect with an assumed tip radius of 10 nm)^[9c] as determined from the AFM images for two of the lowest concentrations. In both cases, the widths of the distributions strongly indicated that even at these low concentrations, **NS1** easily undergoes aggregation, which prevents analysis of the single nanostructures.^[22]

HRTEM: For HRTEM and SAED (selected area electron diffraction) investigations, the solid powder of nanoscaffold

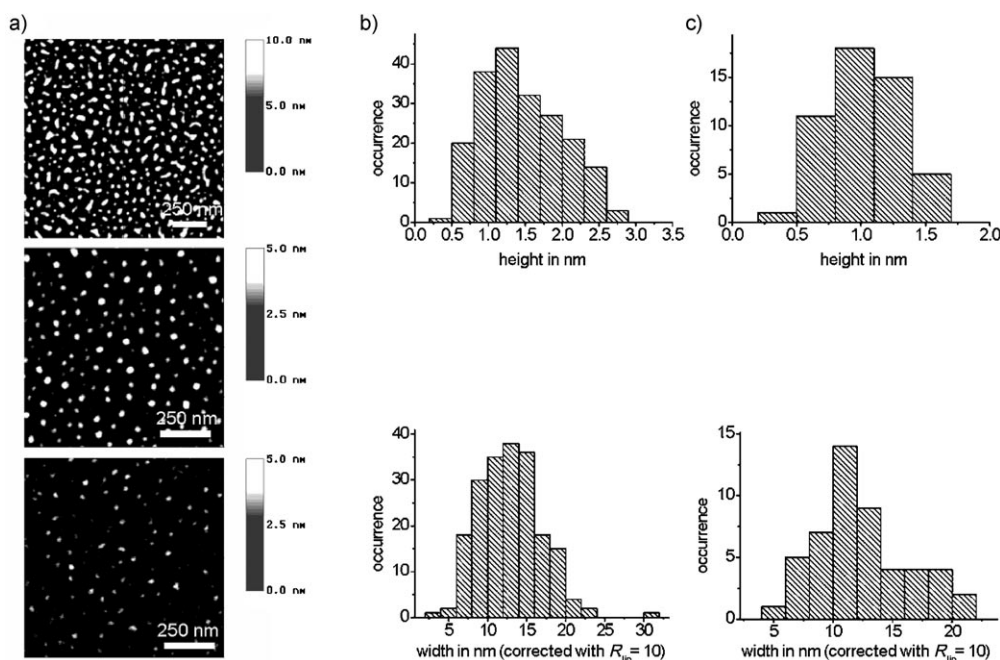


Figure 6. a) Tapping-mode AFM height images of samples of **NS1** spincoated from different concentrations: $\approx 10^{-3}$ M, $\approx 10^{-9}$ M, and $\approx 10^{-10}$ M from top to bottom. b) and c) Histograms of height and width values for samples prepared from concentrations of b) $\approx 10^{-9}$ M, and c) $\approx 10^{-10}$ M.

NS1 was spread on Cu and Al grids or as a solution in acetone on an Al grid (sample 3).^[9c] The use of Al grids was required to improve the appearance of 5 nm sized nanoaggregates, roughly that expected for **NS1** ($d=4.2$ nm). EDX pictures, SAED patterns, HRTEM images, and FFT (fast Fourier transform) spectra of these images proved the presence of copper. The sharp signals of the FFT spectra were located on concentric circles; their diameter corresponded to d_{111} and d_{200} of Cu.^[9c]

Structure elucidation through indirect tests: In the first section, the nanoscaffolds were characterized by standard techniques also used in other labs. In the following, we describe the use of indirect methods, such as chemical oxidation of the nanoscaffolds, size exclusion chromatography, and metal and ligand exchange studies, as well as size selectivity experiments, to interrogate some additional properties of the nanoscaffolds.

Chemical oxidation: **NS1** and **NS2** displayed single reversible waves for the $\text{Cu}^+/\text{Cu}^{2+}$ redox couple in cyclic voltammetry experiments (at $E_{1/2}=1.09$ V_{TPP} and 1.12 V_{TPP} respectively. TPP=triphenylpyrylium), which are in line with the redox potentials of analogous Phen-copper(I)-Phen systems.^[13b,23] Oxidation in combination with ESI-MS can equally be used to interrogate the composition of the aggregates. For this purpose, a mixture of **NS2**^{5+/6+/7+/8+} was generated through the successive addition of tris(*p*-bromophenyl) aminium hexachloroantimonate as a one-electron oxidant to effect the copper(I) to copper(II) oxidation. Depending on the amount of oxidant, the ESI-MS spectra showed all the signals for **NS2**^{5+/6+/7+/8+} (Table 1). The

Table 1. Signals detected by ESI-MS when **NS2**=[Cu₄(**1d**)₂(**2**)₂][PF₆]₄ was oxidized with tris(*p*-bromophenyl)aminium hexachloroantimonate.

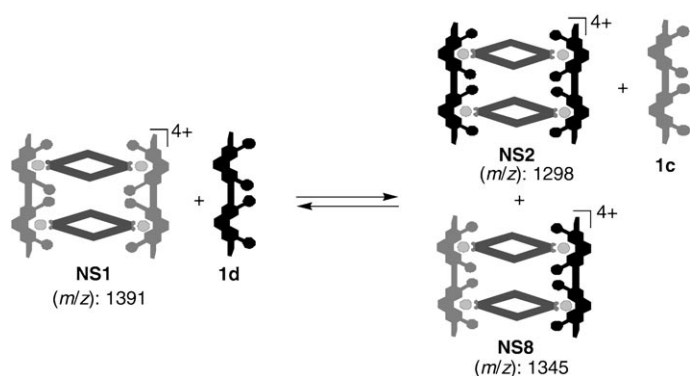
Complex	Calculated mass m/z	Obtained mass m/z (%)
[<i>M</i> -4 PF ₆ +4(Cl ⁻)] ⁴⁺	1333.6	1333.5 (100)
[<i>M</i> -4 PF ₆ +3(Cl ⁻)] ⁴⁺	1324.8	1325.7 (36)
[<i>M</i> -4 PF ₆ +2(Cl ⁻)] ⁴⁺	1315.9	1316.1 (32)
[<i>M</i> -4 PF ₆ +2(TFA ⁻)] ⁴⁺	1307.1	1307.1 (8)
[<i>M</i> -4 PF ₆ +3(TFA ⁻)] ⁴⁺	1354.7	1354.7 (32)
[<i>M</i> -4 PF ₆ +4(TFA ⁻)] ⁴⁺	1383.0	1383.8 (4)

highly charged boxes (>4+) were always associated with chloride ions stemming from the hexachloroantimonate (see Supporting Information). The signals confirm the composition assigned to **NS2**. Most importantly, however, signals of oligomeric complexes could not be detected. These experiments also hint at the potential use of these nanoscaffold structures as redox active hosts for large anionic structures.

Disintegration after size-exclusion chromatography and protonation: When **NS1** was investigated by size-exclusion chromatography various fractions were collected, which contained ligands, metal ions, and combinations thereof, but not **NS1**. Upon combination of all collected fractions, the nanoscaffold **NS1** reformed quantitatively. Along the same line, **NS1** was completely disintegrated by addition of acid, but upon neutralization the nanoscaffold reformed without visible loss.

Ligand exchange studied by ESI-MS: Suitable repair mechanisms are most important in thermochemically controlled protocols towards multicomponent aggregates. Interestingly, such exchange studies have rarely been used to support the

suggested supramolecular structure.^[24] Insight into the exchange reactions of nanoscaffolds **NS1** and **NS2** should therefore provide valuable information about the reversibility of the assembly process and details about relevant intermediates. Hence, we decided to monitor the ligand exchange between **NS1**=[**(1c)**₂(**2**)₂Cu₄]⁴⁺ and added ligand **1d**. Ligand **1d** has the same length and binding properties as **1c**, but a different molecular weight, allowing for a study of the non-self-recognition process by ESI-MS techniques. In an experiment, **1d** and **NS1** were reacted in a 1:1 ratio in dry dichloromethane. Ligand exchange was recognized after 5 min by characteristic signals in the ESI-MS that showed a mixture of three boxes **NS1**, **NS2**, and **NS8**=[**(1c)**(**1d**)(**2**)₂Cu₄]⁴⁺ in *m/z* (%) ratio of 100, 12, and 15, respectively (Scheme 4). All signals corresponding to the scaffolds



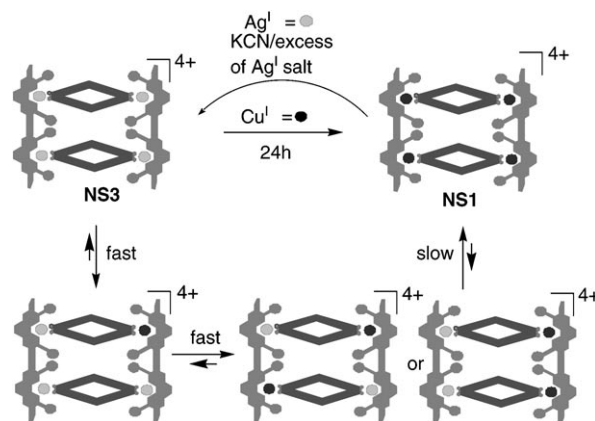
Scheme 4. Schematic representation of products formed in the exchange equilibrium after mixing **NS1** with the linear ligand **1d**.

were isotopically well resolved (see Supporting Information). Similar results were also obtained after addition of two equivalents of **1d** to **NS1** in dichloromethane. In the presence of excess of **1d** (six equivalents with respect to **NS1**) the nanoscaffold disassembled to furnish exclusively the monomeric building blocks.

While these results clearly support the notion of the dynamic nature of the nanoscaffolds **NS1** and **NS2**, the absence of any other hetero nanoscaffold combinations in the ESI-MS further supports the compositions proposed for **NS1**–**NS7**.

Metal exchange studies: Seminal reports by Sauvage and co-workers^[25] have demonstrated the potential of metal exchange to affect motions in catenanes and rotaxanes. However, to date such exchange studies have not been rigorously explored to confirm supramolecular structures or to provide insight into the dynamic processes. Herein, we present the results of a silver–copper exchange reaction in the silver nanoscaffold **NS3**. The **NS3** scaffold was obtained quantitatively by treating **1c** and **2** with AgBF₄ in a 2:2:4 ratio. The composition and structure of **NS3** were confirmed by ESI-MS, ¹H NMR, UV/Vis, and elemental analysis. **NS3** proved to be stable even after exposure to the atmosphere for sev-

eral weeks. As silver(I) bisphenanthroline complexes are known for their lower thermodynamic stability than the corresponding copper(I) complexes, **NS3** was treated with [Cu(MeCN)₄PF₆] or CuI in DCM (see Supporting Information). With CuI in dichloromethane, crucial information about the various intermediates could be extracted smoothly through ESI-MS and UV/Vis spectrometric investigations over a period of 24 h. At 30 min after addition the ESI-MS showed signals corresponding to various species: for example, **NS3** (*m/z* (%) = 100%), [Ag₃Cu(**1c**)₂(**2**)₂]⁴⁺ (27%), [Ag₂Cu₂(**1c**)₂(**2**)₂]⁴⁺ (18%), but almost no [AgCu₃(**1c**)₂(**2**)₂]⁴⁺ and no **NS1**. After about 24 h, **NS1** was the only species present in solution (Supporting Information). During the exchange process it was interesting to observe signals corresponding to the free ligand **1c**, which are absent both in the starting **NS3** and at the endpoint when **NS1** has formed. This observation suggests a dissociation/association mechanism, involving not only metal ions, but also ligands, for this unique exchange process. UV/Vis spectroscopy also provided support for the conversion, as indicated by the appearance of an MLCT band at ≈500 nm typical for copper(I) bisphenanthrolines at the expense of the silver(I) bisphenanthroline complex visible at λ_{max} (sh) = 389 nm. The all silver nanoscaffold **NS3** could be regenerated by treating **NS1** with cyanide and excess silver(I) salt. This interconversion also demonstrates the reversible nature of these assemblies (Scheme 5).

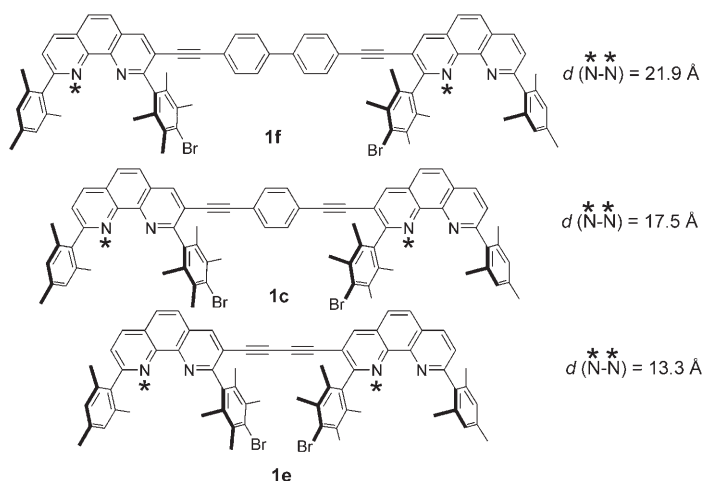


Scheme 5. Cartoon representation of the transmetalation experiment.

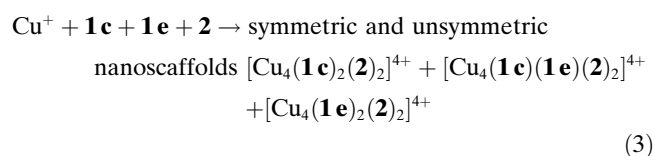
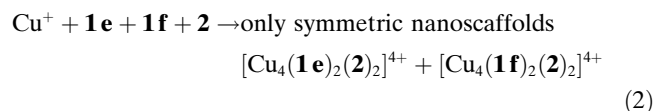
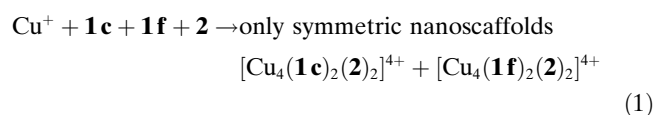
In addition, the exchange process proves that **NS1** and **NS3** must have the suggested composition. If **NS1** or **NS3** had alternative oligomeric structures, such as [(**1c**)_n(**2**)_nM_{2n}]²ⁿ⁺ with *n* > 2, we would have detected mass signals corresponding to higher aggregates [(**1c**)_n(**2**)_nM_{2n-m}M'_m]²ⁿ⁺ during the exchange process. In the absence of any such signals, the present data further support our compositional assignment for the nanoscaffolds **NS1** and **NS3**.

Size selectivity phenomena: It is well documented that a mixture of different ligands can be used for the self-recognition of helicate-type assemblies, for example, leading to the ex-

clusive formation of homoleptic complexes.^[26] Self-recognition can be controlled by the number of metal binding sites or by different spacer lengths. Thus it is a challenge to implement this phenomenon for heteroleptic aggregates for which multiple aggregation scenarios are possible.^[27] Herein, we present a size selectivity study of heteroleptic nanoscaffolds as analyzed by ESI-MS. The ligands **1c**, **1e**, and **1f**



were used for studying the size selection phenomenon. Unfortunately, due to signal overlap, parallel ¹H NMR studies were not suitable. As shown below, the combination of ligands **1f**, **1e** (one equivalent of each) with **2** (two equivalents) in the presence of [Cu(MeCN)₄]PF₆ (four equivalents) in DCM furnished only symmetric scaffolds. Equally, only symmetric aggregates formed when **1c**, **1f**, and **2** were treated with [Cu(MeCN)₄]PF₆. In contrast, from the reaction of **1e**, **1c** and **2** with a Cu(I) salt, both unsymmetric and symmetric combinations were detected [Eqs. (1)–(3)].



ESI-MS titrations: A series of ESI-MS titration experiments was carried out to obtain a qualitative map of the intermediates on the route to the nanoscaffold assembly. Measurements were made only after the spectra were stable with

time, thus assuring that complete thermodynamic equilibrium had been achieved.

ESI-MS titration of 1c/copper(I) with macrocycle 2: In the first series of experiments, **1c** ($8.7 \times 10^{-5} \text{ M}$) and copper(I) ($1.7 \times 10^{-4} \text{ M}$) were titrated with aliquot amounts of **2** in ten additions. Small excess addition of **2** did not affect the nanoscaffold. During the course of the titration, six intermediates were observed apart from the final nanoscaffold. As the titration proceeded, signals corresponding to the nanoscaffold increased, and after the final addition the spectrum contained only signals corresponding to the desired nanoscaffold. All intermediates (see discussion) were clearly identifiable through their *m/z* ratio, their isotopic splitting pattern, and their collisional fragmentation processes. During the titration no oligomeric combinations were detected.

ESI-MS titration of 2/copper(I) with 1c: The second set of experiments was carried out by the titration of **2** and copper(I) salt with aliquot amounts of **1c** in dichloromethane. The analysis of the data indicated that even though [Cu_{*n*}(**2**)₂]^{*n*+} (*n*=1, 2) was present in the initial stage of the titration, these homoleptic structures disassembled to furnish the nanoscaffold assembly as soon as **1c** was added. In this titration, we were able to detect eight intermediates apart from the final nanoscaffold. As the titration proceeded the signals corresponding to the nanoscaffold increased, with the final spectrum only containing signals corresponding to the nanoscaffold.

ESI-MS titration of 2/1c with copper(I): Finally, in a third titration, **2** and **1c** were titrated with copper(I) in dichloromethane. The analysis of the data emphasized the high affinity of **1c** towards metal-ion coordination. Otherwise, the intermediates were the same as in the titrations above. All suggested structures were in accordance with their isotopic splittings. A signal centered at *m/z*=1961 Da was assigned to species **C**. Collisional fragmentation of **D** yielded species **B**, with all signals showing the expected isotopic distributions. Intermediate **B** and the nanoscaffold have the same *m/z* value (1391 Da), but differ in their isotopic splitting. Complex **B** is a 2+ charged species, whereas **E** contains four positive charges. Because of the largely reduced number of intermediates in this titration, this procedure (with copper(I) salt as the titrant) was used for the spectrophotometric titrations (see Figure 7).

Discussion

In the present work we demonstrate how the combination of routine analytical techniques like NMR (¹H and DOSY), UV/Vis, and ESI-MS, complemented by analytical ultracentrifugation, AFM, HRTEM data, and so forth, provide a comprehensive picture of the structure of dynamic heteroleptic oligophenanthroline metallonanoscavolds in solution. Applications of indirect methods, such as chemical interro-

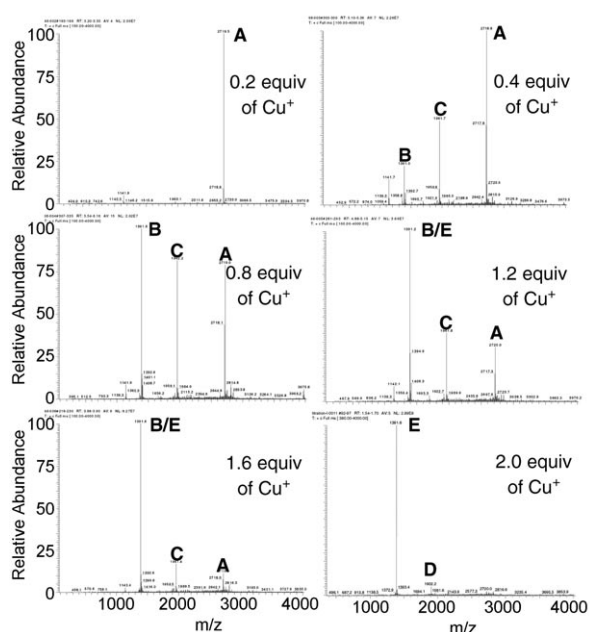


Figure 7. ESI-MS titration of **1c**, **2** with $[\text{Cu}(\text{MeCN})_4]\text{PF}_6$ to furnish **NS1**.

ation of the compounds, size-exclusion chromatography, and ligand-exchange studies, further refine our understanding. In summary, the experiments convincingly indicate that the nanoscaffolds **NS1–NS7** are thermodynamically stable minimum structures with interesting dynamic properties.

Three-dimensional structure: With the failure to produce X-ray data on **NS1–NS7**, MM^+ calculations were performed to visualize the dimensions of the nanoscaffolds.^[28] The space filling models of **NS1**, **NS4**, **NS5**, and **NS6** are displayed in Figure 8. In **NS6**, the external dimensions are ≈ 4.0 nm along the **1g** axis (height), ≈ 3.0 nm (width) and ≈ 5.0 nm for the Cu–Cu diagonal. To the best of our knowledge **NS6** represents the longest tubular discrete architecture (≈ 5.0 nm) reported to date. Unlike the tubular systems reported by Fujita et al.,^[8p] the present systems could be conceived without the addition of any guest as a template, making them potential hosts for biological molecules of comparable size to **NS6**.

Analytical ultracentrifugation results indicate that the mass of the solvated **NS2** is $19.8 \times 10^3 \text{ g mol}^{-1}$, suggesting that the solvation shell of the nanoscaffold involves 240 acetone molecules. Apparently, the solvent accounts for 71% of the overall mass and for 80% of the volume, explaining the low tendency to form crystals suitable for X-ray analysis. The experimental volume of the solvated scaffold **NS2** amounts to $38.8 \times 10^3 \text{ \AA}^3$ agreeing well with the MM^+ calculated volume ($36.2 \times 10^3 \text{ \AA}^3$). The free inner volume ΔV_{in} of **NS1** and **NS2** is important for the design of potential guests. MM^+ calculations predict $\Delta V_{\text{in}} = 6 \times 10^3 \text{ \AA}^3$, suggesting that roughly 50 molecules of acetone fill the inner void.

A piece of important information for understanding whether the structures **NS1–NS7** are floppy or rigid with

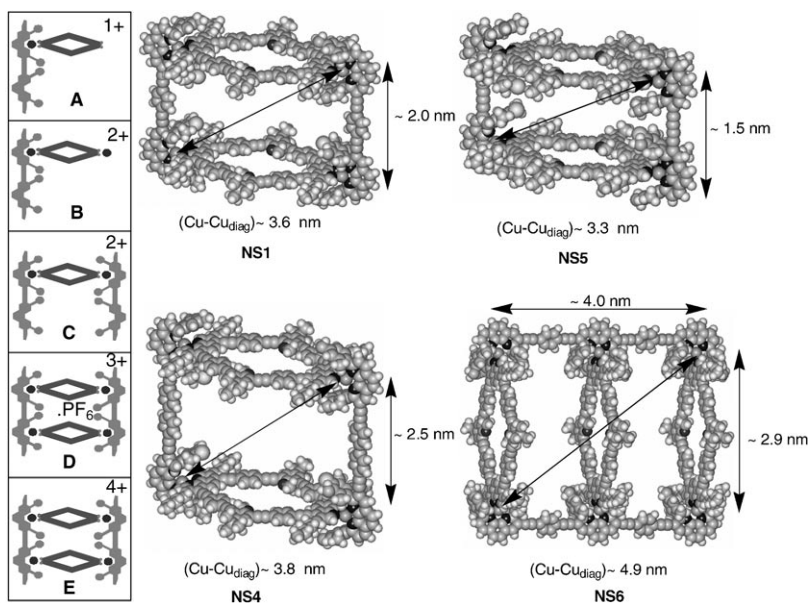


Figure 8. MM^+ -minimized structures of **NS1**, **NS5**, **NS4**, and **NS6** as space-filling representations (Cu–Cu distances are provided).

regard to shear forces or to conformational flexibility is actually delivered by the size selection results in Figure 9. The inability of the system to accommodate the unsymmetrical scaffolds $[\text{Cu}_4(\mathbf{1c})(\mathbf{1f})(\mathbf{2})_2]^{4+}$ and $[\text{Cu}_4(\mathbf{1e})(\mathbf{1f})(\mathbf{2})_2]^{4+}$ is a strong indication of an unpredicted rigidity. Considering macrocycle **2** for the moment as a stiff and inflexible spacer connecting the two opposing linear bisphenanthrolines **1** through copper coordination, it is clear that even small deviations from a coplanar arrangement of the two macrocycles in **NS** are energetically penalized (Figure 9). Only very minor differences in the lengths of the two linear bisphenanthrolines, such as in **1c** and **1e**, are energetically acceptable to afford the unsymmetric nanoscaffold. Simple calculations propose that with an angle of up to 4.1° , enclosed by the two macrocycles, unsymmetric scaffolds such as $[\text{Cu}_4(\mathbf{1c})(\mathbf{1e})(\mathbf{2})_2]^{4+}$ still form. In the experimentally inaccessible structure $[\text{Cu}_4(\mathbf{1c})(\mathbf{1f})(\mathbf{2})_2]^{4+}$ the angle is 4.4° . It is worth stating that even in these experiments no homoleptic combinations were found. Again, the non-self-recognition of the ligands during the formation of the nanoscaffolds is reliably controlled by the HETPHEN concept.

All our efforts to elucidate the structures of **NS1–NS7** by techniques such as STM, AFM, and HRTEM were met with failure. While STM measurements were not successful at all, the AFM studies only depicted aggregates, presumably composed of multiples of **NS**. HRTEM, in contrast, seemed to be successful at first glance, as nanoaggregates of the correct size were discovered. Further investigation of the nanoparticles, however, revealed that they consisted of pure copper, as their structure agreed with the fcc structure of bulk copper.^[9c] Apparently, the last method only works in selected cases under special conditions.^[29]

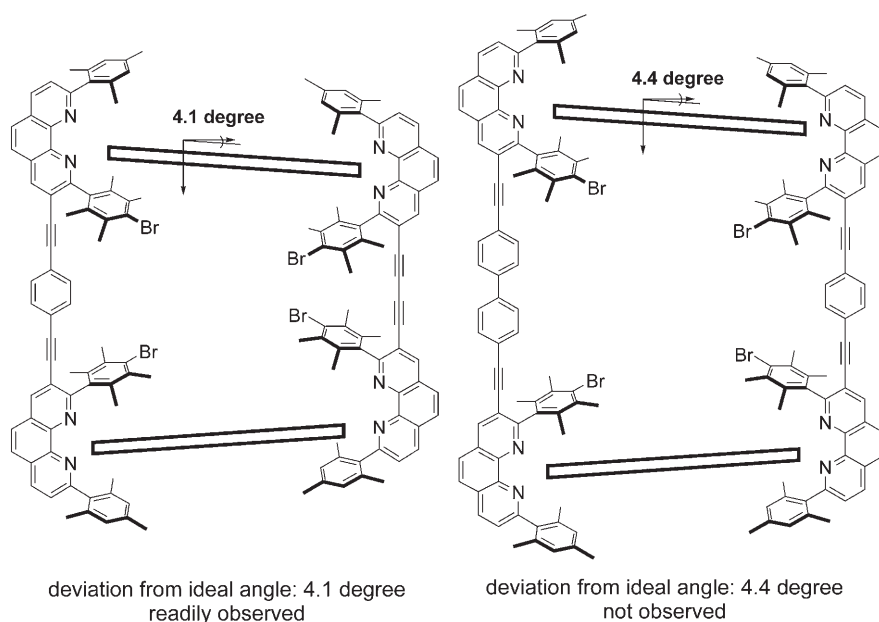
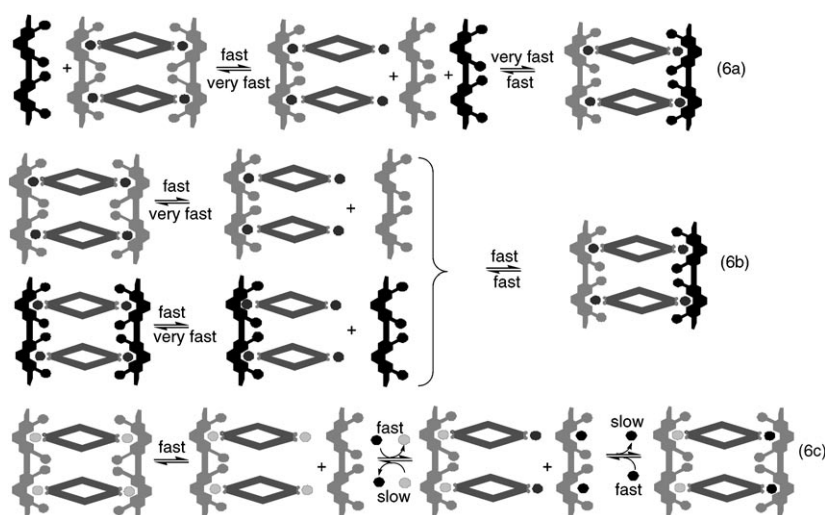


Figure 9. Cartoon representation of the deviation from the ideal angle in the unsymmetric scaffolds $[\text{Cu}_4(\mathbf{1c})-(\mathbf{1e})(\mathbf{2})_2]^{4+}$ (left) and $[\text{Cu}_4(\mathbf{1c})(\mathbf{1f})(\mathbf{2})_2]^{4+}$ (right) obtained from model calculations assuming a stiff macrocycle **2**.

Dynamics: The characterization of a thermochemically stable system is not complete without some insight into its dynamic nature. The experiments above indicate that the exchange of a linear bisphenanthroline in **NS1** takes place within minutes, while the exchange of metal ions proceeds much more slowly, that is, on the timescale of several hours. In principle, two competing hypotheses are reasonable to explain the fast exchange of a linear ligand and the slow exchange of metal ions. In the first hypothesis (Scheme 6) the complete dissociation of a linear bisphenanthroline is con-

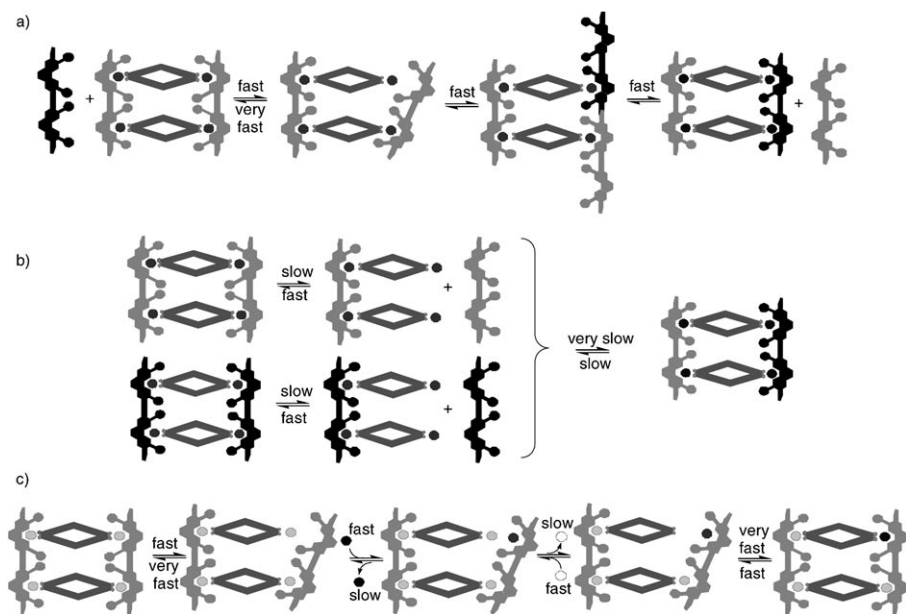
sidered to be a fast step as indicated in Scheme 6a. This model makes the prediction that the kinetic exchange of ligands between two different nanoscaffolds should still be rapid (Scheme 6b), but that metal exchange due to the need for liberation of some of the coordination sites from metal ions is slow (last step in Scheme 6c). Experimentally, the exchange of ligands after mixing the two nanoscaffolds **NS1** and **NS2** is negligible, and even after hours no unsymmetric scaffold is formed. This finding clearly disagrees with first hypothesis. The second hypothesis suggests that full dissociation of the bisphenanthroline is slow, but that partial dissociation at one bisdiimine coordination site is kinetically rapid. This allows the incoming linear bisphenanthroline to attach rapidly, thus preventing the reformation of the original scaffold (Scheme 7a). As the concentration of free bisphenanthroline is rather low, this model predicts very slow ligand exchange upon mixing of the nanoscaffolds (Scheme 7b) and slow exchange of metal ions (Scheme 7c), as was found experimentally.

The assembly process: Mechanistic investigations should provide a deeper understanding of the basic principles of non-self-assembly versus self-assembly processes, which is



Scheme 6. Cartoon representation of the dynamics according to hypothesis 1: dissociation of **1** at both metal binding sites is fast. a) The fast ligand exchange in the presence of a second linear bisphenanthroline. b) Ligand exchange between two different nanostructures. It is fast due to an acceptable equilibrium concentration of free linear bisphenanthrolines. c) Slow metal ion exchange in presence of added metal ions.

urgently required for the design of systems of higher complexity and functionality. As two different ligands assemble by means of metal coordination during the formation of heteroleptic nanoscaffolds the non-self-recognition interactions must be dominant. Since one of the ligands used in this study, **2**, is able to form a homoleptic assembly in competition, the quantitative formation of a heteroleptic nanoscaffold should be the result of cooperativity. Very few reports about mechanistic pathways of self-assembled systems are at hand, and investigations into nanoscale assemblies are even more rare.^[30] The **NS1** assembly was chosen for a detailed study by using a



Scheme 7. Cartoon representation of the dynamics according to hypothesis 2: dissociation of **1** at one metal binding site is fast. a) Fast ligand exchange in the presence of a second linear bisphenanthroline. b) Ligand exchange between two different nanostructures. It is very slow due to the low equilibrium concentration of free linear bisphenanthrolines. c) Slow metal ion exchange in the presence of added metal ions.

combination of ESI-MS and spectrophotometric titrations. Whereas the ESI-MS studies provided qualitative information about possible intermediates, the spectrophotometric titrations, processed by SPECFIT,^[31–33] allowed determination of the thermodynamic parameters for the intermediates and the final nanoscaffold. Measurements were carried out in dichloromethane, for solubility reasons and to avoid any competitive coordination with the solvent.^[34]

At the beginning of the various titration protocols (vide supra), the mechanism and emerging intermediates are evidently dominated by the starting conditions (starting compounds vs. titrant). If we start with macrocycle **2** in the presence of copper(I), initially homoleptic complexes of the kind $[\text{Cu}_m(\mathbf{2})_n]^{m+}$ are solely detected. Immediately upon addition of **1c**, however, the copper(I) ions are only found associated with the linear bisphenanthroline. This is a general observation for these titrations. Of the two ligands, **1c** is found associated preferentially with the metal ion, probably due to stabilizing cation– π interactions between the metal ion and the aromatic groups in the 2,9-positions. Such a finding does not contradict our mechanistic suggestion in Schemes 6 and 7. It indicates, however, that the association of the metal ion with macrocycle **2** instead of with **1c–h**, as needed for some of the ligand and metal exchange reactions, requires an addition small endergonic step.

Clearly, the titrations show a very simple non-self-assembly process involving only a limited number of key intermediates. Hence, a cartoon description of the assembly process is depicted in Scheme 8. Apart from $[\text{Cu}_m(\mathbf{2})_n]^{m+}$, the same key intermediates were observed in all three titrations. All the signals were in good agreement with their isotopic splittings.

Conclusion

As it is rather difficult to obtain single crystals from nanoscaffolds larger than ≈ 3 nm containing large voids it is highly important to utilize several solution characterization techniques to ascertain the proposed supramolecular structures. Herein, we present the preparation of nanoscaffolds, some of which have a tubular shape, and a battery of methods for their characterization in solution. The assemblies possessing unprecedented voids are unambiguously characterized by several spectroscopic means and control experiments. Metal and ligand exchange studies demonstrate the reversibility of the assemblies, and the absence of any indication of other oligomeric combinations further supports the proposed nanostructures.

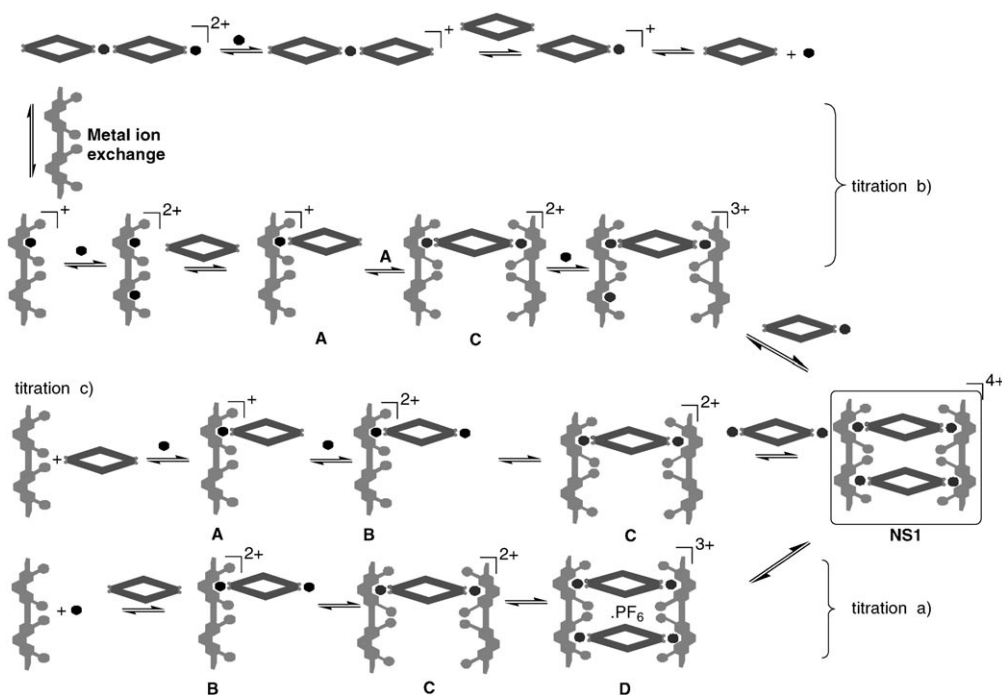
Silver and copper nanoscaffolds can be interconverted readily with no homoleptic complexes formed in between. Mechanistic insight into these assemblies as gained through ESI-MS titrations leads to a better understanding of the processes occurring during the formation of **NSI**, which should be a model case for all heteroleptic nanoscale assemblies of this investigation. Mechanistically, the assembly protocols proved to be strikingly similar, independent of the addition sequence, except for the starting situation. A four-step pathway is postulated for the assembly of the nanoscaffold in the ESI-MS titration of **2/copper(I)** with **1c**. Even the two main intermediates are formed only in minor amounts and rapidly convert to the final nanoscaffold.

In conclusion, we present an efficient strategy for heteroleptic supramolecular nanoscale assemblies and outline a series of solution-state techniques to characterize dynamic metallosupramolecular aggregates with large internal voids. The large voids make them attractive host systems for nanoscopic guest molecules.

Experimental Section

Ligands **1a–h** were prepared according to known procedures.^[15] ¹H NMR and ¹³C NMR were measured on a Bruker AC 200 (200 MHz) or Bruker Avance 400 (400 MHz). All ¹H NMR measurements were carried at room temperature in deuterated dichloromethane unless otherwise specified. $[\text{Cu}(\text{MeCN})_4]\text{PF}_6$ was prepared according to the known procedures.^[35]

Ligand 1h: Yield 74%; mp > 300 °C; ¹H NMR (400 MHz, [D]chloroform, 25 °C): δ = 8.45 (s, 2H), 8.44 (s, 2H), 8.28 (d, J = 8.0 Hz, 2H), 7.89 (d, J = 8.8 Hz, 2H), 7.85 (s, 2H), 7.83 (d, J = 9.0 Hz, 2H), 7.57 (d, J = 8.0 Hz,



Scheme 8. Cartoon representation of the detected intermediates in the formation of nanoscaffold NS1. Titration a): **1c**+copper(I) is titrated with **2**. Titration b): **2**+copper(I) is titrated with **1c**. Titration c): **1c**+**2** is titrated with copper(I).

2H), 7.04 (d, $J=8.4$ Hz, 4H), 6.96 (d, $J=8.4$ Hz, 4H), 6.93 (s, 4H), 6.92 (s, 4H), 2.45 (s, 12H), 2.36 (s, 6H), 2.31 (s, 6H), 2.11 (s, 12H), 2.07 (s, 12H), 2.00 ppm (s, 12H); ^{13}C NMR (CDCl_3 , 100 MHz): $\delta=162.52$, 162.48, 160.7, 145.9, 144.9, 144.8, 139.1, 138.4, 138.3, 138.0, 137.5, 137.4, 136.8, 136.2, 136.1, 135.8, 133.7, 133.6, 131.5, 131.3, 129.1, 128.5, 128.0, 127.6, 127.3, 127.2, 126.9, 126.5, 125.6, 125.3, 122.9, 122.7, 119.9, 119.8, 95.1, 94.8, 89.3, 89.0, 21.2, 21.1, 20.9, 20.6, 20.1, 18.6 ppm; IR (KBr): $\tilde{\nu}=2918$, 1614, 1504, 1452 cm^{-1} ; ESI-MS: m/z (%): 1680.8 (100) $[\text{M}+1]^+$ (calcd for $\text{C}_{112}\text{H}_{90}\text{Br}_2\text{N}_6$: 1679.8), 841.1 (24) $[\text{M}+2]^{2+}$ (calcd for $\text{C}_{112}\text{H}_{90}\text{Br}_2\text{N}_6$: 839.9); elemental analysis calcd (%) for $\text{C}_{112}\text{H}_{90}\text{Br}_2\text{N}_6 \cdot 2\text{H}_2\text{O}$: C 78.40, H 5.52, N 4.90; found: C 78.26, H 5.31, N 4.91.

General procedure for the formation of nanoscaffold motifs (NS1–7): Nanoscaffolds NS1–5 were prepared by mixing **1c–1f** and **2** with $[\text{Cu}(\text{MeCN})_4]\text{PF}_6$ or AgBF_4 (2:2:4 equivalents) in dichloromethane. The resulting dark red solution (yellow color solution in the case of NS3) was analyzed by ESI-MS, ^1H and ^{13}C NMR spectroscopy, and elemental analysis without any further purification. Using the same procedure NS6 and NS7 were prepared by reacting **1g,h**, **2** and $[\text{Cu}(\text{MeCN})_4]\text{PF}_6$ (2:3:6 equivalents) in dichloromethane.

Spectrophotometric titrations: UV/Vis spectra were recorded on a Tidas II spectrophotometer by using dichloromethane as the solvent. Equilibrium constants of the complexes were determined in dichloromethane. Ligands **1c** and **2** were titrated with aliquot amounts of a stock solution of the copper(I) tetrakisacetonitrile hexafluorophosphate. All stock solutions were prepared by careful weighing on a μg analytical balance. Absorption spectra were recorded at $25.0 \pm (0.1)^\circ\text{C}$. Since the formation is instantaneous, as evident from proton NMR spectroscopy, ESI-MS analysis, and color change, the solutions were immediately analyzed to avoid problems with the volatile solvent. The wavelength region from 240 to 600 nm was taken into account. Stoichiometrically adequate equivalents of the metal salt in dichloromethane were added in 20 portions. The entire data sets, comprising the 240 to 600 nm absorbances, measured in one nanometer resolution, were decomposed into their principal components by factor analysis, and subsequently the formation constants, including their standard deviations, were calculated using the SPECFIT^[31]

program. Binding constants were determined from two independent titrations.

ESI-MS investigations: Positive ESI-MS spectra were recorded on the LCQ Deca Thermo Quest instrument, scanning over the m/z range 200–4000. Each time a total of 25 scans were accumulated for the final spectrum. The samples were introduced in the ESI source at a flow rate of 10 mL min^{-1} . Typical ESI-MS conditions used in this study: the sheath gas flow rate, spray voltage, capillary voltage, and tube lens offset were set at 50 (arb), 5 kV, 200 $^\circ\text{C}$, 41 V, and 5 V, respectively, in order to avoid any fragmentation. Assignment of the signals was further confirmed by comparison of their isotopic splitting with calculated values and also by additional collisional fragmentations.

NS1 ($[\text{Cu}_4(\mathbf{1c})_2(\mathbf{2})_2]^{4+}$): M.p. 295–298 $^\circ\text{C}$; ^1H NMR (400 MHz, $[\text{D}_2]$ dichloromethane, 25 $^\circ\text{C}$): $\delta=8.81$ (s, 4H; phenanthroline), 8.63 (d, $J=7.6$ Hz, 4H; phenanthroline), 8.45 (s, 8H; phenanthroline), 8.28 (s, 8H; phenanthroline), 8.20 (d, $J=9.2$ Hz, 4H; phenanthroline), 8.17 (d, $J=9.2$ Hz 4H; phenanthroline), 7.81 (d, $J=7.8$ Hz, 4H; phenanthroline), 7.69 (d, $J=8.2$ Hz, 16H; phenyl), 7.64 (d, $J=8.2$ Hz, 16H; phenyl), 7.54 (s, 8H; phenyl), 6.92 (s, 8H; phenyl), 5.96 (s, 8H; Mes-H), 4.16 (s, 12H; methoxy), 2.98 (m, 16H; aliph), 1.71 (s, 24H; benzyl), 1.64 (s, 12H; aliph), 1.54 (s, 24H; benzyl), 1.47 (s, 24H; aliph), 1.31 (s, 36H; *t*Bu), 0.77 ppm (t, $J=7.2$ Hz, 24H; aliph); ^{13}C NMR (CDCl_3 , 200 MHz): $\delta=163.4$, 161.6, 160.1, 148.9 (2C), 146.2, 145.8, 144.4, 143.4 (2C), 138.9, 137.9, 137.5, 136.2, 135.4 (2C), 134.9 (2C), 134.2, 133.6, 133.1, 132.5, 132.0, 131.8, 131.3, 129.8 (2C), 129.1, 128.5, 128.2, 127.6, 127.3, 126.9, 126.5, 126.3 (2C), 126.0, 125.6, 125.0, 122.8, 121.6, 119.0, 109.1, 96.2 (arom), 93.8 (2C), 89.9 (2C), 88.6 (2C), 84.4 (2C) (ethynyl), 62.8 (methoxy), 34.1, 32.6, 31.8, 31.0, 30.2, 29.6, 22.5, 21.8, 21.2 (2C), 20.9 (2C), 20.2 (2C), 13.5 ppm (aliph); IR (KBr): $\tilde{\nu}=2926$, 2840, 2194 ($\text{C}\equiv\text{C}$), 1598, 1507, 1460, 1422, 1291, 1160, 1110, 1005, 842, 678, 548 cm^{-1} ; ESI-MS: m/z (%): 1391.5 (100) $[\text{M}]^{4+}$ (calcd for $[\text{Cu}_4\text{C}_{364}\text{H}_{328}\text{N}_{16}\text{Br}_4\text{O}_4\text{PF}_6]^{4+}$: 1391.1), 1903.0 (5) $[\text{M}]^{3+}$ (calcd for $[\text{Cu}_4\text{C}_{364}\text{H}_{328}\text{N}_{16}\text{Br}_4\text{O}_4\text{PF}_6]^{3+}$: 1903.1); elemental analysis calcd (%) for $\text{Cu}_4\text{C}_{364}\text{H}_{328}\text{N}_{16}\text{Br}_4\text{O}_4 \cdot 4\text{PF}_6 \cdot 2\text{CD}_2\text{Cl}_2$: C 69.58, H 5.36, N 3.55; found: C 69.44, H 5.48, N 3.52.

NS2 ($[\text{Cu}_4(\mathbf{1d})_2(\mathbf{2})_2]^{4+}$): M.p. 280 $^\circ\text{C}$; ^1H NMR (400 MHz, $[\text{D}_2]$ Dichloromethane, 25 $^\circ\text{C}$): $\delta=8.86$ (s, 4H; phenanthroline), 8.70 (d, $J=7.8$ Hz, 4H; phenanthroline), 8.51 (s, 8H; phenanthroline), 8.38 (s,

8H; phenanthroline), 8.24 (d, $J=9.6$ Hz, 4H; phenanthroline), 8.21 (d, $J=9.6$ Hz 4H; phenanthroline), 7.84 (d, $J=7.8$ Hz, 4H; phenanthroline), 7.82 (d, $J=8.2$ Hz, 16H; phenyl), 7.74 (d, $J=8.2$ Hz, 16H; phenyl), 7.60 (s, 8H; phenyl), 7.17 (s, 8H; phenyl), 6.10 (s, 8H; Mes-H), 5.99 (s, 8H; Mes-H), 4.23 (s, 12H; methoxy), 3.09 (t, $J=6.9$ Hz, 16H; aliph), 1.80–1.90 (m, 16H; aliph), 1.72 (s, 48H; aliph), 1.67 (s, 12H; benzyl), 1.64 (s, 12H; benzyl), 1.45–1.60 (m, 16H; aliph), 1.37 (s, 36H; *t*Bu), 1.30–1.42 (m, 32H; aliph), 0.88 ppm (t, $J=7.2$ Hz, 24H; aliph); IR (KBr): $\tilde{\nu}=2922$, 2848, 2194 (C=C), 1591, 1509, 1460, 1419, 1296, 1166, 1102, 1002, 838, 681, 552 cm^{-1} ; ESI-MS: m/z (%): 1298.1 (100) $[M]^{4+}$ (calcd for $[\text{Cu}_4\text{C}_{360}\text{H}_{324}\text{N}_{16}\text{O}_4]^{4+}$: 1298.2), 1778.1 (20) $[M]^{3+}$ (calcd for $[\text{Cu}_4\text{C}_{360}\text{H}_{324}\text{N}_{16}\text{O}_4\text{PF}_6]^{3+}$: 1778.2); elemental analysis calcd (%) for $\text{Cu}_4\text{C}_{360}\text{H}_{324}\text{N}_{16}\text{O}_4\text{PF}_6\cdot 1.5\text{CD}_2\text{Cl}_2$: C 73.55, H 5.63, N 3.80; found: C 73.59, H 6.35, N 3.80.

NS3 ($[\text{Ag}_4(\mathbf{1c})(\mathbf{2})_2]^{4+}$): M.p. $>300^\circ\text{C}$; ^1H NMR (400 MHz, $[\text{D}_2]$ dichloromethane, 25°C): $\delta=8.77$ (s, 4H; phenanthroline), 8.60 (d, $J=7.6$ Hz, 4H; phenanthroline), 8.55 (s, 8H; phenanthroline), 8.28 (s, 8H; phenanthroline), 8.15 (d, $J=9.2$ Hz, 4H; phenanthroline), 8.13 (d, $J=9.2$ Hz 4H; phenanthroline), 7.84 (d, $J=7.8$ Hz, 4H; phenanthroline), 7.69 (d, $J=8.2$ Hz, 16H; phenyl), 7.65 (d, $J=8.2$ Hz, 16H; phenyl), 7.54 (s, 8H; phenyl), 6.92 (s, 8H; phenyl), 5.96 (s, 8H; Mes-H), 4.16 (s, 12H; methoxy), 2.98 (m, 16H; aliph), 1.86 (s, 24H; benzyl), 1.81 (s, 12H; aliph), 1.61 (s, 24H; benzyl), 1.55 (s, 24H; benzyl), 1.31 (s, 36H; *t*Bu), 0.82 ppm (t, $J=7.2$ Hz, 24H; benzyl); ^{13}C NMR (CDCl_3 , 200 MHz): $\delta=165.4$, 162.6, 159.1, 149.1, 146.7, 145.4, 144.9, 143.4 (2C), 138.9, 137.9, 137.5, 136.2, 135.4 (2C), 134.9 (2C), 135.3, 133.9, 133.4, 132.9, 132.0, 131.5, 131.2, 130.5 (2C), 129.3, 128.5, 128.0, 127.6, 127.3, 126.9, 126.5, 126.3 (2C), 126.0, 125.6, 125.0, 122.0, 121.6, 116.5, 107.5, 95.2 (arom), 93.8 (2C), 88.9 (2C), 87.1 (2C), 82.4 (2C) (ethynyl), 60.8 (methoxy), 35.9, 33.6, 31.4, 30.8, 29.7, 28.6, 22.0, 21.8, 21.2 (2C), 20.9 (2C), 19.5 (2C), 12.5 ppm (aliph); IR (KBr): $\tilde{\nu}=2936$, 2852, 2198 (C=C), 1598, 1515, 1460, 1419, 1296, 1166, 1102, 1002, 838, 681, 552 cm^{-1} ; ESI-MS: m/z (%): 1435.2 (100) $[M]^{4+}$ (calcd for $[\text{Ag}_4\text{C}_{360}\text{H}_{328}\text{N}_{16}\text{Br}_4\text{O}_4]^{4+}$: 1435.2); elemental analysis calcd (%) for $\text{Ag}_4\text{C}_{360}\text{H}_{328}\text{N}_{16}\text{Br}_4\text{O}_4\cdot 4\text{BF}_4\cdot 5\text{CD}_2\text{Cl}_2$: C 67.94, H 5.38, N 3.44; found: C 67.98, H 5.31, N 3.46.

NS4 ($[\text{Cu}_4(\mathbf{1f})(\mathbf{2})_2]^{4+}$): ^1H NMR (200 MHz, $[\text{D}_2]$ dichloromethane, 25°C): $\delta=8.83$ (s, 4H; phenanthroline), 8.73 (d, $J=8.3$ Hz, 4H; phenanthroline), 8.53 (s, 8H; phenanthroline), 8.34 (s, 8H; phenanthroline), 8.22 (d, $J=9.1$ Hz, 8H; phenanthroline), 7.93 (d, $J=8.1$ Hz, 4H; phenanthroline), 7.83 (d, $J=8.1$ Hz, 16H; phenyl), 7.74 (d, $J=8.3$ Hz, 16H; phenyl), 7.61 (s, 8H; phenyl), 7.55 (d, $J=8.6$ Hz, 8H; phenyl), 7.43 (d, $J=8.6$ Hz, 8H; phenyl), 6.11 (s, 8H; Mes-H), 4.24 (s, 12H; methoxy), 3.01–3.18 (m, 16H; aliph), 1.83 (s, 48H; benzyl), 1.63 (s, 36, benzyl), 1.35–1.37 (m, 100H; aliph), 0.89 ppm (t, $J=6.6$ Hz, 24H; aliph); ^{13}C NMR (CDCl_3 , 50 MHz): $\delta=166.2$, 158.7, 154.6, 153.9, 147.9, 147.1, 143.9, 142.1, 141.2, 140.6, 138.3, 138.1, 134.5, 133.2 (2C), 132.2, 131.9 (2C), 130.6, 130.3, 129.7, 128.6 (2C), 128.4 (2C), 128.0, 127.7, 125.8, 125.6 (2C), 125.1, 124.0, 121.6 (2C), 120.6, 119.8, 119.0, 116.5, (arom), 93.8 (2C), 84.5 (2C), 81.6 (2C), 84.8 (2C) (ethynyl), 64.3 (methoxy), 32.7, 31.6 (2C), 30.9 (2C), 29.2 (2C), 28.2, 23.9, 22.6 (2C), 13.8 ppm (aliph); ESI-MS: m/z (%): 1429.4 (100) $[M]^{4+}$ (calcd for $[\text{Cu}_4\text{C}_{376}\text{H}_{336}\text{Br}_4\text{N}_{16}\text{O}_4]^{4+}$: 1429.1).

NS5 $[\text{Cu}_4(\mathbf{1e})(\mathbf{2})_2]^{4+}$: m.p. 289°C ; ^1H NMR (200 MHz, $[\text{D}_2]$ Dichloromethane, 25°C): $\delta=8.83$ (s, 4H; phenanthroline), 8.73 (d, $J=8.1$ Hz, 4H; phenanthroline), 8.52 (s, 8H; phenanthroline), 8.33 (s, 8H; phenanthroline), 8.22 (q, $J=9.1$ Hz, 4H; phenanthroline), 8.10 (s, 4H; phenanthroline), 7.92 (d, $J=8.4$ Hz, 4H; phenanthroline), 7.89 (s, 8H; phenyl), 7.83 (d, $J=8.3$ Hz, 16H; phenyl), 7.74 (d, $J=8.3$ Hz, 16H; phenyl), 7.61 (s, $J=8.2$ Hz, 8H; phenyl), 6.10 (s, 8H; Mes-H), 4.23 (s, 12H; methoxy), 3.12 (t, $J=7.9$ Hz, 16H; aliph), 2.29 (m, 4H; aliph), 1.82 (s, 36H; benzyl), 1.63 (s, 48H; benzyl), 1.36 (s, 36H; *t*Bu), 0.88 ppm (t, $J=6.9$ Hz, 32H; aliph); ^{13}C NMR (100 MHz, CD_2Cl_2): $\delta=160.6$, 159.8, 159.2, 147.7, 146.8, 143.3, 142.4, 140.9, 140.5, 140.3, 138.1, 137.8, 137.3, 137.0, 134.2, 132.9, 131.9, 131.6 (2C), 131.0, 128.7, 128.2, 127.7, 127.4, 127.2, 126.8, 126.7, 125.8, 125.2, 124.8, 121.3, 121.1, 116.2, 104.4 (arom), 92.4 (2C), 88.3 (2C), 84.6 (2C), 84.5 (2C) (ethynyl), 61.4 (methoxy), 34.1, 32.4, 31.3, 30.6, 30.5, 28.9, 22.3, 19.9, 19.6, 19.5, 17.7, 13.5 ppm (aliph); ESI-MS: m/z (%): 1354.1 (100) $[M]^{4+}$ (calcd for $[\text{Cu}_4\text{C}_{352}\text{H}_{320}\text{N}_{16}\text{O}_4\text{Br}_4]^{4+}$: 1353.1), 1852.8 (14) $[M]^{3+}$ (calcd for $[\text{Cu}_4\text{C}_{352}\text{H}_{320}\text{N}_{16}\text{O}_4\text{Br}_4\text{PF}_6]^{3+}$: 1852.4).

NS6 ($[\text{Cu}_6(\mathbf{1g})(\mathbf{2})_3]^{6+}$): M.p. $>300^\circ\text{C}$; ^1H NMR (400 MHz, $[\text{D}_2]$ dichloromethane, 25°C): $\delta=8.83$ (s, 4H; phenanthroline), 8.80 (s, 4H; phenanthroline), 8.74 (d, $J=7.8$ Hz, 4H; phenanthroline), 8.51 (s, 12H; phenanthroline), 8.37 (s, 12H; phenanthroline), 8.22 (d, $J=9.6$ Hz, 4H; phenanthroline), 8.19 (d, $J=9.6$ Hz, 4H; phenanthroline), 8.13 (s, 4H; phenyl), 7.70–7.90 (m, 52H; phenyl), 7.61 (s, 12H; phenyl), 6.99 (s, 16H; phenyl), 6.06 (s, 16H; Mes-H), 5.97 (s, 8H; Mes-H), 4.25 (s, 18H; methoxy), 3.09 (t, $J=6.9$ Hz, 24H; aliph), 2.00 (s, 24H; benzyl), 1.80–1.90 (m, 16H; aliph), 1.92 (s, 48H; benzyl), 1.79 (s, 12H; benzyl), 1.75 (s, 12H; benzyl), 1.71 (s, 12H; benzyl), 1.45–1.60 (m, 24H; aliph), 1.37 (s, 54H; *t*Bu), 1.30–1.42 (m, 48H; aliph), 0.87 ppm (t, $J=7.2$ Hz, 36H; aliph); IR (KBr): $\tilde{\nu}=2922$, 2854, 2192 (C=C), 1598, 1510, 1460, 1420, 1398, 1293, 1245, 1162, 1104, 1004, 838, 739, 558 cm^{-1} ; ESI-MS: m/z 1318.4 (22) $[M]^{6+}$ (calcd (%) for $[\text{Cu}_6\text{C}_{550}\text{H}_{488}\text{N}_{24}\text{O}_6]^{6+}$: 1318.5), 1611.5 (92) $[M]^{3+}$ (calcd for $[\text{Cu}_6\text{C}_{550}\text{H}_{488}\text{N}_{24}\text{O}_6\text{PF}_6]^{3+}$: 1611.2), 2051.3 (100) $[M]^{4+}$ (calcd (%) for $[\text{Cu}_6\text{C}_{550}\text{H}_{488}\text{N}_{24}\text{O}_6\cdot 2\text{PF}_6]^{4+}$: 2050.2), 2783.1 (36) $[M]^{3+}$ (calcd (%) for $[\text{Cu}_6\text{C}_{550}\text{H}_{488}\text{N}_{24}\text{O}_6\cdot 3\text{PF}_6]^{3+}$: 2782.0); elemental analysis calcd. (%) for $\text{Cu}_6\text{C}_{550}\text{H}_{488}\text{N}_{24}\text{O}_6\cdot 10\text{CD}_2\text{Cl}_2$: C 69.70, H 5.51, N 3.48; found: C 69.83, H 5.73, N 3.43.

NS7 ($[\text{Cu}_6(\mathbf{1h})(\mathbf{2})_3]^{6+}$): M.p. $>300^\circ\text{C}$; ^1H NMR (400 MHz, $[\text{D}_2]$ tetrachloroethane, 25°C): $\delta=8.89$ (s, 4H; phenanthroline), 8.87 (s, 4H; phenanthroline), 8.77–8.70 (m, 4H; phenanthroline), 8.48 (s, 12H; phenyl), 8.32 (s, 12H; phenyl), 8.25–8.15 (m, 12H; phenanthroline), 7.93–7.89 (m, 4H; phenanthroline), 7.86–7.72 (m, 36H; phenyl), 7.58 (s, 12H; phenyl), 7.11–7.06 (m, 16H; phenyl), 6.02–5.99 (16H; Mes-H), 4.22 (s, 18H; methoxy), 1.80 (s, 24H; benzyl), 1.74 (s, 24H; benzyl), 1.68 (s, 24H; benzyl), 1.58 (s, 24H; benzyl), 1.55 (s, 12H; benzyl), 1.51 (s, 12H; benzyl), 1.49–1.45 (m, 24H; benzyl), 1.42–1.31 (m, 48H; aliph), 1.26 (s, 54H; *t*Bu), 0.89–0.87 ppm (m, 36H; aliph); IR (KBr): $\tilde{\nu}=2921$, 2851, 2195 (C=C), 1598, 1510, 1460, 1421, 1398, 1244, 1162, 1103, 1015, 840, 741, 558 cm^{-1} ; ESI-MS: m/z (%): 1380.2 (100) $[M]^{6+}$ (calcd for $[\text{Cu}_6\text{C}_{554}\text{H}_{492}\text{Br}_4\text{N}_{24}\text{O}_6]^{6+}$: 1380.5), 1685.2 (49) $[M]^{3+}$ (calcd for $[\text{Cu}_6\text{C}_{554}\text{H}_{492}\text{Br}_4\text{N}_{24}\text{O}_6\text{PF}_6]^{3+}$: 1685.6), 2143.1 (10) $[M]^{4+}$ (calcd for $[\text{Cu}_6\text{C}_{554}\text{H}_{492}\text{Br}_4\text{Cu}_6\text{N}_{24}\text{O}_6\cdot 2\text{PF}_6]^{4+}$: 2143.2), 2903.3 (4) $[M]^{3+}$ (calcd for $[\text{Cu}_6\text{C}_{554}\text{H}_{492}\text{Br}_4\text{N}_{24}\text{O}_6\cdot 3\text{PF}_6]^{3+}$: 2903.9); elemental analysis calcd (%) for $\text{Cu}_6\text{C}_{554}\text{H}_{492}\text{Br}_4\text{N}_{24}\text{O}_6\cdot 11\text{C}_2\text{D}_2\text{Cl}_4$: C 62.77, H 4.90, N 3.05; found: C 62.85, H 5.20, N 2.98.

Acknowledgements

We are grateful to the Deutsche Forschungsgemeinschaft, the SFB 448 (J.P.R.), the Alexander von Humboldt Foundation (P.M.) and the Fonds der Chemischen Industrie for financial support. V.K. thanks Dr. Anne-Marie Albrecht-Gary (Strasbourg) for help with the Scatchard plot fitting.

- [1] a) *Comprehensive Supramolecular Chemistry, Vols. 1–11* (Eds.: J.-M. Lehn, J. L. Atwood, J. E. D. Davis, D. D. MacNicol, F. Vögtle), Pergamon, Oxford (UK), **1996**; b) M. Schmittel, V. Kalsani, *Top. Curr. Chem.* **2005**, *245*, 1–53.
- [2] a) S. R. Seidel, P. J. Stang, *Acc. Chem. Res.* **2002**, *35*, 972–983, and references therein; b) Y. K. Kryschenko, S. R. Seidel, D. C. Muddiman, A. I. Nepomuceno, P. J. Stang, *J. Am. Chem. Soc.* **2003**, *125*, 9647–9652; c) P. S. Mukherjee, N. Das, P. J. Stang, *J. Org. Chem.* **2004**, *69*, 3526–3529; d) M. Schweiger, T. Yamamoto, P. J. Stang, D. Blaser, R. Boese, *J. Org. Chem.* **2005**, *70*, 4861–4864.
- [3] a) C. M. Drain, J.-M. Lehn, *J. Chem. Soc. Chem. Commun.* **1994**, 2313–2315; b) P. N. W. Baxter, J.-M. Lehn, G. Baum, D. Fenske, *Chem. Eur. J.* **1999**, *5*, 102–112; c) A. M. Garcia, D. M. Bassani, J.-M. Lehn, G. Baum, D. Fenske, *Chem. Eur. J.* **1999**, *5*, 1234–1238.
- [4] a) G. R. Newkome, T. J. Cho, C. N. Moorefield, G. R. Baker, R. Cush, P. S. Russo, *Angew. Chem.* **1999**, *111*, 3899–3903; *Angew. Chem. Int. Ed.* **1999**, *38*, 3717–3721; b) G. R. Newkome, T. J. Cho, C. N. Moorefield, R. Cush, P. S. Russo, L. A. Godinez, M. J. Saunders, P. Mohapatra, *Chem. Eur. J.* **2002**, *8*, 2946–2954; c) G. R.

- Newkome, T. J. Cho, C. N. Moorefield, P. Mohapatra, L. A. Godinez, *Chem. Eur. J.* **2004**, *10*, 1493–1500; d) P. Wang, C. N. Moorefield, G. R. Newkome, *Angew. Chem.* **2005**, *117*, 1707–1711; *Angew. Chem. Int. Ed.* **2005**, *44*, 1679–1683; e) S.-H. Hwang, C. N. Moorefield, F. R. Fronczek, O. Lukoyanova, L. Echevoyen, G. R. Newkome, *Chem. Commun.* **2005**, 713–715.
- [5] a) V. Paraschiv, M. Crego-Calama, R. H. Fokkens, C. J. Padberg, P. Timmerman, D. N. Reinhoudt, *J. Org. Chem.* **2001**, *66*, 8297–8301; b) L. J. Prins, E. E. Neuteboom, V. Paraschiv, M. Crego-Calama, P. Timmerman, D. N. Reinhoudt, *J. Org. Chem.* **2002**, *67*, 4808–4820; c) V. Paraschiv, M. Crego-Calama, T. Ishi-i, C. J. Padberg, P. Timmerman, D. N. Reinhoudt, *J. Am. Chem. Soc.* **2002**, *124*, 7638–7639.
- [6] M. Fujita, M. Tominaga, A. Hori, B. Therrien, *Acc. Chem. Res.* **2005**, *38*, 369–378, and references therein.
- [7] a) R. Takahashi, Y. Kobuke, *J. Am. Chem. Soc.* **2003**, *125*, 2372–2373; b) Y. Kuramochi, A. Satake, Y. Kobuke, *J. Am. Chem. Soc.* **2004**, *126*, 8668–8669.
- [8] a) R. Ziessel, *Synthesis* **1999**, 1839–1865; b) F. Würthner, A. Sautter, *Chem. Commun.* **2000**, 445–446; c) S. C. Johannessen, R. G. Brisbois, *J. Am. Chem. Soc.* **2001**, *123*, 3818–3819; d) R. D. Sommer, A. L. Rheingold, A. J. Goshe, B. Bosnich, *J. Am. Chem. Soc.* **2001**, *123*, 3940–3952; e) A. Sautter, D. G. Schmid, G. Jung, F. Würthner, *J. Am. Chem. Soc.* **2001**, *123*, 5424–5430; f) S. S. Sun, A. J. Lees, *Inorg. Chem.* **2001**, *40*, 3154–3160; g) F. Würthner, A. Sautter, D. Schmid, P. G. A. Weber, *Chem. Eur. J.* **2001**, *7*, 894–902; h) M. L. Merlau, M. P. Mejia, S. T. Nguyen, J. T. Hupp, *Angew. Chem.* **2001**, *113*, 4369–4372; *Angew. Chem. Int. Ed.* **2001**, *40*, 4239–4242; i) H. Fenniri, B. L. Deng, A. E. Ribbe, *J. Am. Chem. Soc.* **2002**, *124*, 11064–11072; j) H. Fenniri, B. L. Deng, A. E. Ribbe, K. Hallenga, J. Jacob, P. Thiagarajan, *Proc. Natl. Acad. Sci. USA* **2002**, *99*, 6487–6492; k) F. Würthner, A. Sautter, *Org. Biomol. Chem.* **2003**, *1*, 240–243; l) C. C. You, F. Würthner, *J. Am. Chem. Soc.* **2003**, *125*, 9716–9725; m) H. Jiang, W. Lin, *J. Am. Chem. Soc.* **2003**, *125*, 8084–8085; n) H. Jiang, W. Lin, *J. Am. Chem. Soc.* **2004**, *126*, 7426–7427; o) T. Yamaguchi, S. Tashiro, M. Tominaga, M. Kawano, T. Ozeki, M. Fujita, *J. Am. Chem. Soc.* **2004**, *126*, 10818–10819; p) C. A. Schalley, *Angew. Chem.* **2004**, *116*, 4499–4501; *Angew. Chem. Int. Ed.* **2004**, *43*, 4399–4401; q) M. Tominaga, K. Suzuki, M. Kawano, T. Kusukawa, T. Ozeki, S. Sakamoto, K. Yamaguchi, M. Fujita, *Angew. Chem.* **2004**, *116*, 5739–5743; *Angew. Chem. Int. Ed.* **2004**, *43*, 5621–5625; r) S.-L. Zheng, M. Gembicky, M. Messerschmidt, P. M. Dominiak, P. Coppens, *Inorg. Chem.* **2006**, *45*, 9281–9289; s) P. P. Bose, M. G. B. Drew, A. K. Das, A. Banerjee, *Chem. Commun.* **2006**, 3196–3198; t) T. D. Nguyen, K. C.-F. Leung, M. Liong, C. D. Pentecost, J. F. Stoddart, J. I. Zink, *Org. Lett.* **2006**, *8*, 3363–3366.
- [9] a) D. G. Kurth, N. Severin, J. P. Rabe, *Angew. Chem.* **2002**, *114*, 3833–3835; *Angew. Chem. Int. Ed.* **2002**, *41*, 3681–3683; b) V. Kalsani, H. Ammon, F. Jäckel, J. P. Rabe, M. Schmittel, *Chem. Eur. J.* **2004**, *10*, 5481–5492; c) M. Schmittel, V. Kalsani, L. Kienle, *Chem. Commun.* **2004**, 1534–1535, and references therein; d) M. Schmittel, V. Kalsani, F. Jäckel, J. P. Rabe, J. W. Bats, D. Fenske, *Eur. J. Org. Chem.* **2006**, *14*, 3079–3086; e) F. P. Seebeck, K. J. Woycechowsky, W. Zhuang, J. P. Rabe, D. Hilvert, *J. Am. Chem. Soc.* **2006**, *128*, 4516–4517.
- [10] Y. Cohen, L. Avram, L. Frish, *Angew. Chem.* **2005**, *117*, 524–560; *Angew. Chem. Int. Ed.* **2005**, *44*, 520–554.
- [11] D. Schubert, C. Tziatzios, P. Schuck, U. S. Schubert, *Chem. Eur. J.* **1999**, *5*, 1377–1383.
- [12] a) C. T. Seto, G. M. Whitesides, *J. Am. Chem. Soc.* **1993**, *115*, 905–916; b) J. C. Nelson, K. G. Saven, J. S. Moore, P. G. Wolynes, *Science* **1997**, *277*, 1793–1796; c) I. Higler, L. Grave, E. Breuning, W. Verboom, F. De Jong, T. M. Fyles, D. N. Reinhoudt, *Eur. J. Org. Chem.* **2000**, 1727–1734.
- [13] HETPHEN concept: a quantitative approach to heteroleptic bisphenanthroline metal complexes. This approach utilizes steric and electronic effects originating from bulky aryl substituents at the bisimine coordination sites to control the coordination equilibrium both kinetically and thermodynamically; a) M. Schmittel, A. Ganz, *Chem. Commun.* **1997**, 999–1000; b) M. Schmittel, U. Lüning, M. Meder, A. Ganz, C. Michel, M. Herderich, *Heterocycl. Commun.* **1997**, *3*, 493–498; c) M. T. Miller, P. K. Gantzel, T. B. Karpishin, *J. Am. Chem. Soc.* **1999**, *121*, 4292–4293; d) M. Schmittel, H. Ammon, V. Kalsani, A. Wiegrefe, C. Michel, *Chem. Commun.* **2002**, 2566–2567.
- [14] a) A. Harriman, J.-P. Sauvage, *Chem. Soc. Rev.* **1996**, *25*, 41–48; b) C. Dietrich-Buchecker, G. Rapenne, J.-P. Sauvage, *Coord. Chem. Rev.* **1999**, *185–186*, 167–176.
- [15] a) M. Schmittel, C. Michel, A. Wiegrefe, V. Kalsani, *Synthesis* **2001**, 1561–1567; b) M. Schmittel, C. Michel, A. Wiegrefe, *Synthesis* **2005**, 367–373.
- [16] a) V. Goulle, R. P. Thummel, *Inorg. Chem.* **1990**, *29*, 1767–1772; b) X. Y. Li, J. Illigen, M. Nieger, S. Michel, C. A. Schalley, *Chem. Eur. J.* **2003**, *9*, 1332–1347.
- [17] M. Schmittel, V. Kalsani, D. Fenske, A. Wiegrefe, *Chem. Commun.* **2004**, 490–491.
- [18] a) C. O. Dietrich-Buchecker, P. A. Marnot, J.-P. Sauvage, J. R. Kirchoff, D. R. McMillin, *J. Chem. Soc. Chem. Commun.* **1983**, 513–515; b) N. Fatin-Rouge, S. Blanc, A. Pfeil, A. Rigault, A. M. Albrecht-Gary, J.-M. Lehn, *Helv. Chim. Acta* **2001**, *84*, 1694–1711.
- [19] K. C. Russell, E. Leize, A. VanDorselaer, J.-M. Lehn, *Angew. Chem.* **1995**, *107*, 244–248; *Angew. Chem. Int. Ed. Engl.* **1995**, *34*, 209–213.
- [20] a) E. N. G. Marsh, W. F. DeGrado, *Proc. Natl. Acad. Sci. USA* **2002**, *99*, 5150–5154; b) M. Rasa, U. S. Schubert, *Soft Matter*, **2006**, *2*, 561–572.
- [21] I. Gössl, L. Shu, A. D. Schlüter, J. P. Rabe, *J. Am. Chem. Soc.* **2002**, *124*, 6860–6865.
- [22] It seems not to be useful to dilute further, because, already at the lowest concentration used, very large uncovered substrate areas were found. This might be due to adsorption of the molecules to the substrate after the de-wetting of the solvent film during spin-coating. Thus, it will be increasingly difficult to find covered areas at further dilution. Secondly, the height images at the lowest concentration used demonstrate that we approach the limits of the instrument.
- [23] I. Poleschak, J. M. Kern, J.-P. Sauvage, *Chem. Commun.* **2004**, 474–476, and references therein.
- [24] a) P. N. W. Baxter, *Comprehensive Supramolecular Chemistry*, Vol. 9 (Eds.: J.-M. Lehn, J. L. Atwood, J. E. D. Davis, D. D. MacNicol, F. Vögtle), **1996**, Chapter 5, pp. 165–211; b) B. Olenyuk, A. Fechtenkötter, P. J. Stang, *J. Chem. Soc. Dalton. Trans.* **1998**, *11*, 1707–1728; c) S. Leininger, B. Olenyuk, P. J. Stang, *Chem. Rev.* **2000**, *100*, 853–907.
- [25] M. C. Jimenez-Molero, C. Dietrich-Buchecker, J. P. Sauvage, *Chem. Commun.* **2003**, 1613–1616, and references therein.
- [26] a) R. Kramer, J.-M. Lehn, A. Marquis-Rigault, *Proc. Natl. Acad. Sci. USA* **1993**, *90*, 5394–5398; b) M. Albrecht, O. Blau, R. Fröhlich, *Proc. Natl. Acad. Sci. USA* **2002**, *99*, 4867–4872; c) D. L. Caulder, K. N. Raymond, *Angew. Chem.* **1997**, *109*, 1508–1510; *Angew. Chem. Int. Ed. Engl.* **1997**, *36*, 1440–1442; d) M. Albrecht, O. Blau, E. Wegelius, K. Rissanen, *New J. Chem.* **1999**, *23*, 667–668.
- [27] K. Addicott, N. Das, P. J. Stang, *Inorg. Chem.* **2004**, *43*, 5335–5338.
- [28] Molecular modelling was done with the MM + force field as implemented in Hyperchem 6.02. Hyperchem 6.02 Release for Windows by Hypercube, Inc. **2000**. MM + force field.
- [29] T. Premkumar, K. E. Geckeler, *Small* **2006**, *2*, 616–620.
- [30] M. D. Levin, P. J. Stang, *J. Am. Chem. Soc.* **2000**, *122*, 7428–7429.
- [31] a) F. J. C. Rossotti, H. S. Rossotti, R. J. Whewell, *J. Inorg. Nucl. Chem.* **1971**, *33*, 2051–2065; b) H. Gampp, M. Maeder, C. J. Meyer, A. D. Zuberbühler, *Talanta* **1985**, *32*, 95–101; c) H. Gampp, M. Maeder, C. J. Meyer, A. D. Zuberbühler, *Talanta* **1985**, *32*, 257–264; d) H. Gampp, M. Maeder, C. J. Meyer, A. D. Zuberbühler, *Talanta* **1986**, *33*, 943–951. SPECFIT uses the factor analysis to reduce the absorption matrix and to extract the eigenvectors prior to the multiwavelength fit of the reduced data set according to the Marquardt algorithm.^[32] Models that do not fit in the data are rejected. From the obtained association constants distribution curves were computed using the Halthafall program.^[33]

- [32] a) D. W. Marquardt, *J. Soc. Ind. Appl. Math.* **1963**, *11*, 431–441;
b) M. Maeder, A. D. Zuberbühler, *Anal. Chem.* **1990**, *62*, 2220–2224.
- [33] N. Ingri, W. Kakolowicz, L. G. Sillen, B. Warnqvist, *Talanta* **1967**, *14*, 1261–1286.
- [34] a) R. Stiller, J.-M. Lehn, *Eur. J. Inorg. Chem.* **1998**, 977–982.
- [35] G. J. Kubas, *Inorg. Synth.* **1979**, *19*, 90–92.

Received: January 5, 2007
Published online: May 16, 2007